Article

Cancer Cell

CXCR2 Inhibition Profoundly Suppresses Metastases and Augments Immunotherapy in Pancreatic Ductal Adenocarcinoma

Graphical Abstract

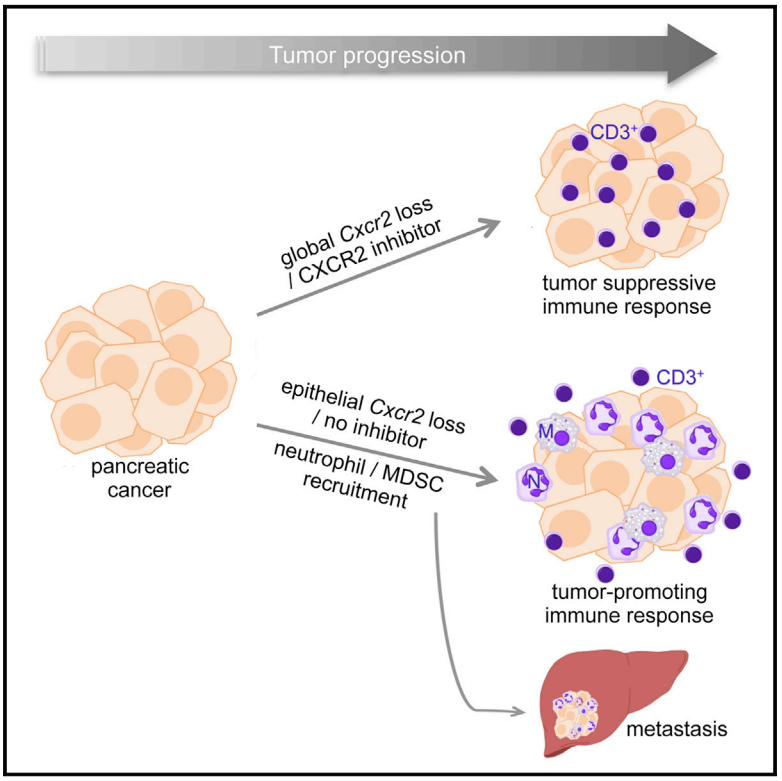

Authors

Colin W. Steele, Saadia A. Karim, Joshua D.G. Leach, ..., Simon T. Barry, Owen J. Sansom, Jennifer P. Morton

Correspondence

o.sansom@beatson.gla.ac.uk

In Brief

Steele et al. show that CXCR2 is important in immune modulation of pancreatic cancer and that inhibition of CXCR2 reduces metastasis and improves response to gemcitabine and anti-PD1. Peptide inhibitor, but not germline deletion of *Cxcr2*, improved survival, revealing differential effects in early and late tumors.

Highlights

- CXCR2 signaling is upregulated in myeloid cells in human pancreatic cancer
- *Cxcr2* loss reduces metastasis and inhibition prolongs tumor-free survival in mice
- Neutrophils/MDSCs play a key role in the establishment of the metastatic niche
- CXCR2 inhibition enhances T cell entry and confers sensitivity to anti-PD1 therapy

Accession Numbers

E-MTAB-4659

Steele et al., 2016, Cancer Cell *29*, 832–845
June 13, 2016
http://dx.doi.org/10.1016/j.ccell.2016.04.014

CellPress

CellPress

Cancer Cell
Article

CXCR2 Inhibition Profoundly Suppresses Metastases and Augments Immunotherapy in Pancreatic Ductal Adenocarcinoma

Colin W. Steele,[1] Saadia A. Karim,[1] Joshua D.G. Leach,[1] Peter Bailey,[2] Rosanna Upstill-Goddard,[2] Loveena Rishi,[2] Mona Foth,[1] Sheila Bryson,[1] Karen McDaid,[3] Zena Wilson,[3] Catherine Eberlein,[3] Juliana B. Candido,[4] Mairi Clarke,[5] Colin Nixon,[1] John Connelly,[1] Nigel Jamieson,[6] C. Ross Carter,[6] Frances Balkwill,[4] David K. Chang,[2] T.R. Jeffry Evans,[1,2] Douglas Strathdee,[1] Andrew V. Biankin,[2] Robert J.B. Nibbs,[5] Simon T. Barry,[3] Owen J. Sansom,[1,2,7,*] and Jennifer P. Morton[1,2,7]

[1]Cancer Research UK Beatson Institute, Garscube Estate, Switchback Road, Glasgow G61 1BD, UK
[2]Institute of Cancer Sciences, University of Glasgow, Glasgow G61 1BD, UK
[3]Oncology iMED, AstraZeneca, Alderley Park, Macclesfield SK10 4TG, UK
[4]Centre for Cancer and Inflammation, Barts Cancer Institute, London EC1M 6BQ, UK
[5]Institute of Infection, Immunity and Inflammation, University of Glasgow, Glasgow G12 8QQ UK
[6]Department of Surgery, Glasgow Royal Infirmary, Glasgow G4 0SF, UK
[7]Co-senior author
*Correspondence: o.sansom@beatson.gla.ac.uk
http://dx.doi.org/10.1016/j.ccell.2016.04.014

SUMMARY

CXCR2 has been suggested to have both tumor-promoting and tumor-suppressive properties. Here we show that CXCR2 signaling is upregulated in human pancreatic cancer, predominantly in neutrophil/myeloid-derived suppressor cells, but rarely in tumor cells. Genetic ablation or inhibition of CXCR2 abrogated metastasis, but only inhibition slowed tumorigenesis. Depletion of neutrophils/myeloid-derived suppressor cells also suppressed metastasis suggesting a key role for CXCR2 in establishing and maintaining the metastatic niche. Importantly, loss or inhibition of CXCR2 improved T cell entry, and combined inhibition of CXCR2 and PD1 in mice with established disease significantly extended survival. We show that CXCR2 signaling in the myeloid compartment can promote pancreatic tumorigenesis and is required for pancreatic cancer metastasis, making it an excellent therapeutic target.

INTRODUCTION

Pancreatic ductal adenocarcinoma (PDAC) is an almost universally lethal malignancy and represents a significant therapeutic challenge (http://info.cancerresearchuk.org/cancerstats). Gemcitabine has been the standard of care for patients since 1997, despite offering only marginal benefit (Burris et al., 1997). Recent improvements in survival using FOLFIRINOX and gemcitabine plus nab-paclitaxel have offered a choice to clinicians for the first time (Conroy et al., 2011; Goldstein et al., 2015). However, the 5-year survival rate remains ~6%. Surgical resection is the only potential cure; however, only 15% of patients are suitable for surgery, and most die within 2 years of surgery due to recurrence or metastatic disease. Thus, a greater understanding of how key molecular and cellular regulators of tumor progression combine to drive invasion and metastases in PDAC is required.

Pancreatic cancer develops and metastasizes as a result of the accumulation of multiple genetic and epigenetic changes. Activating mutations of the *KRAS* proto-oncogene occur in >90% of cases (Almoguera et al., 1988), while inactivation of tumor

Significance

PDAC is predicted to become the second commonest cause of cancer death in the United States by 2020. Aggressive invasion and early metastases are characteristic of the disease, and even the few patients eligible for potentially curative resection inevitably develop recurrent or metastatic disease. Early indications suggest that immunotherapy will not work in unselected pancreatic cancer patients. Our data highlight two therapeutic opportunities for PDAC: first the use of CXCR2 inhibitors in surgically resected patients, and second the use of CXCR2 inhibition in combination with immunotherapy in surgically unresectable advanced disease. Our data also suggest that therapeutic targets that may cause senescence escape will not have deleterious effects in late-stage disease in PDAC, because tumors have already escaped this checkpoint.

suppressor genes, including *CDKN2A*, *TP53*, *SMAD4*, and *BRCA2* accrue throughout disease development (Hruban et al., 2000). Progression is a complex process and is reliant on interactions between the tumor and its microenvironment (Baumgart et al., 2013). Ubiquitous to all PDAC is the dense desmoplastic stroma, consisting of immune cells, stellate cells, fibroblasts, and a dense extracellular collagenous matrix, which surrounds PDAC cells, providing vital signals for survival, tumor cell invasion, and metastasis (Olive et al., 2009). However, two recent studies found that targeting the stroma led to accelerated disease progression (Ozdemir et al., 2014; Rhim et al., 2014), although both approaches provided opportunities for immune-targeting therapies. Indeed, targeting FAP^+ fibroblasts in pancreatic tumor-bearing mice can synergize with anti-programmed death 1 (anti-PD1) immunotherapy to cause tumor regression (Feig et al., 2013). Thus, there may be a complex interplay of tumor-promoting and tumor-suppressive consequences when targeting specific pathways.

The relationship between inflammation and PDAC progression is complex. Initially PDAC must overcome immune surveillance; indeed, both human and mouse pancreatic intraepithelial neoplasia (PanINs) and PDAC are characterized by the infiltration of immune suppressor cells, suggesting tumor immunity is blocked early during tumorigenesis (Clark et al., 2007). Once immune surveillance has been bypassed, the net effect of interactions between tumor and immune cells is PDAC progression. However, certain cell types may have the capacity for tumor suppression and promotion in different contexts. For example, inflammatory signaling can promote oncogene-induced senescence (Acosta et al., 2008; Kuilman et al., 2008). On the other hand, inflammation can drive pancreatic tumorigenesis: there is enhanced tumorigenesis in mice subjected to pancreatitis (Guerra et al., 2007), and patients with hereditary pancreatitis have a greatly increased risk of PDAC (Lowenfels et al., 1997). More recently, specific inflammatory signaling pathways, such as STAT3/IL-6 (Baumgart et al., 2014; Corcoran et al., 2011; Fukuda et al., 2011; Lesina et al., 2011), NF-κB (Daniluk et al., 2012; Ling et al., 2012; Maniati et al., 2011), and CXCR2 (Ijichi et al., 2011; Matsuo et al., 2009a) have been implicated in PDAC progression.

CXCR2 is a G-protein-coupled receptor for the human CXC chemokines CXCL1, CXCL2, CXCL3, CXCL5, CXCL6, CXCL7, and CXCL8. Mouse CXCR2 has a more limited repertoire of ligands because mice lack *CXCL6* and *CXCL8* genes. The primary immune function of CXCR2 is the regulation of neutrophil migration, as it controls the egress of these cells from the bone marrow, and their recruitment to sites of inflammation (Cacalano et al., 1994; Eash et al., 2010). CXCR2 also regulates the migration of myeloid-derived suppressor cells (MDSCs) (Highfill et al., 2014). We have previously shown that CXCR2 is fundamental to the process of tumorigenesis in both colon and skin (Jamieson et al., 2012). However, there is growing evidence that CXCR2 is also important for the metastatic process. For example, *Cxcr2* deletion can reduce the invasive and metastatic potential of lung cancer cells (Saintigny et al., 2013). In models of breast cancer, CXCR2 signaling is important for attracting $Gr\text{-}1^+$ $CD11b^+$ MDSCs to the tumor microenvironment, where they drive invasion and metastasis (Yang et al., 2008). Moreover, CXCL1/2 secretion at metastatic sites can promote the establishment of a metastatic niche by enhancing the influx of MDSCs (Acharyya et al., 2012). Indeed, neutrophils have recently been shown to support metastatic colonization by breast cancer cells (Wculek and Malanchi, 2015).

There is emerging evidence for a role of neutrophils, MDSCs, and CXCR2 in pancreatic cancer. Neutrophil infiltration is observed in pancreatic tumors with the poorest prognosis (Reid et al., 2011), while high levels of the CXCR2 ligand CXCL5 are associated with poorer survival and, by implication, metastatic disease (Li et al., 2011). Recent studies have described the contribution of MDSCs to pancreatic cancer progression (Bayne et al., 2012), and the accumulation of MDSCs in patients with advanced pancreatic cancer correlates with disease stage (Diaz-Montero et al., 2009). Moreover, in vitro experiments and transplants in immunodeficient animals have implicated CXCR2 in the regulation of pancreatic tumor cell proliferation, invasion, and angiogenesis (Matsuo et al., 2009a, 2009b; Purohit et al., 2016; Wang et al., 2013). CXCR2 inhibition has also been shown to disrupt interactions between tumor cells and fibroblasts to slow tumor progression in a mouse model of pancreatic cancer, although the mice used exhibit high levels of stromal deregulation and are short lived (Ijichi et al., 2011). These tumor-promoting properties of CXCR2 may be counterbalanced by CXCR2-dependent tumor-suppressing activities. Of particular relevance to PDAC, are the elegant studies that show that CXCR2 reinforces RAS-mediated senescence in culture, and regulates the senescence-associated secretory phenotype (Acosta et al., 2008). We therefore sought here to determine the role of CXCR2 signaling in pancreatic tumorigenesis using relevant in vivo models.

RESULTS

CXCR2 Signaling at the Tumor Border Is Associated with Poor Outcome in Human PDAC

To investigate the importance of CXCR2 in human pancreatic cancer we analyzed the expression of *CXCR2* and its ligands in samples from a cohort of 44 PDAC patients. RNA was prepared from targeted biopsies of tumor borders, and from the adjacent normal pancreas, and chemokine and *CXCR2* expression examined. We found that genes encoding *CXCR2*, and two of its ligands, *CXCL2* and *CXCL8*, were significantly upregulated compared with adjacent normal pancreas (Figure 1A), and high *CXCR2* or *CXCL2* expression was associated with significantly poorer prognosis (Figure 1B). High *CXCR2* expression was also associated with advanced T stage ($p = 0.05$), tumor grade ($p = 0.037$), and resection margin status ($p = 0.015$). We next examined CXCR2 protein by immunohistochemistry (IHC) on full-face sections taken from the edges of tumors adjacent to normal tissue, and found that high expression was associated with poor outcome (Figure 1C). Rather than being expressed in the tumor, most of the observed CXCR2 staining was within the stroma (Figure 1D). Further analysis of the cells present at these areas revealed high numbers of myeloperoxidase (MPO)-positive cells indicating the presence of neutrophils or their precursors (Figure 1D). There was a significant correlation between expression of MPO and CXCR2 in the stroma at the edge of these tumors adjacent to normal regions (Spearman's rho 0.907, $p = 0.01$).

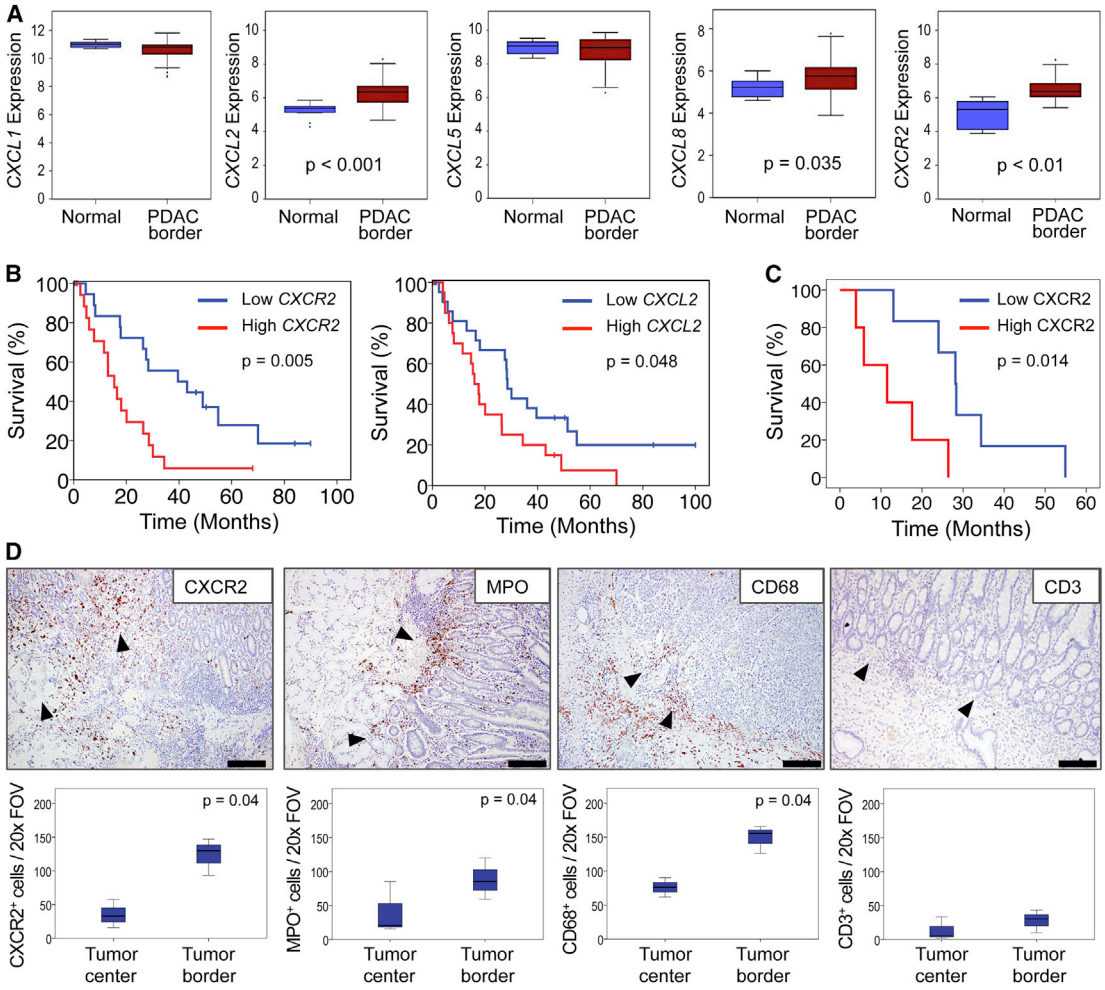

Figure 1. CXCR2 Expression at the Tumor Border Is Associated with Poor Outcome in Human PDAC

(A) Expression of *CXCR2* and its ligands in the tumor border compared with adjacent normal pancreas within pancreaticoduodenectomy specimens (n = 44). RNA was prepared from whole targeted biopsies of the edges of tumors, post-resection, and from adjacent normal pancreas. p Values, Mann-Whitney U test.

(B) Kaplan-Meier analysis of survival in terms of low or high *CXCR2* and *CXCL2* expression from RNA from whole targeted biopsies of the edges of resected tumors. p Values, log rank test.

(C) Kaplan-Meier analysis of survival in terms of low or high CXCR2 expression as assessed by IHC on full-face sections of tumor border regions (n = 11). p Values, log rank test.

(D) IHC staining for CXCR2, MPO, CD68, and CD3 in the stroma at the edge of resected tumors. Arrowheads indicate direction of invasion into either adjacent duodenum or normal pancreas. Scale bars represent 500 μm. Boxplots below show quantification of cells staining positive for each marker in the tumor center versus tumor border (n ≥ 3). p Values, Mann-Whitney U test. The region 1 mm proximal to the adjacent normal tissue was assessed in (C and D). See also Figure S1.

There were also high numbers of $CD68^+$ macrophages, but few $CD3^+$ T cells: these cells were, however, observed in the tissue surrounding the tumors (Figure 1D).

Interestingly, the association of CXCR2-positive cells with prognosis appeared to depend on their location. When we examined tissue from the tumor body (Figure S1A), neither stromal nor tumor epithelial CXCR2 expression was associated with survival (Figure S1B). These data show that the effects of CXCR2 signaling, and recruitment of myeloid cells, differ depending on the site to which these cells are recruited. It is clear, however, that CXCR2 signaling and myeloid cell recruitment at the tumor border are linked to poor outcome in patients. Importantly, very few tumor cells expressed CXCR2.

KPC Mice Recapitulate the Microenvironment and CXCR2 Expression Profile of Human PDAC

In order to further investigate the importance of CXCR2 signaling in PDAC we used a mouse model that both phenotypically and histologically recapitulates the human disease. KPC (*LSL-Kras*$^{G12D/+}$; *LSL-Trp53*$^{R172H/+}$; *Pdx1-Cre*) mice carry a pancreas-specific *Trp53*^{R172H} mutation alongside an initiating mutation in *Kras*^{G12D}, and develop invasive, metastatic tumors that exhibit an extensive stroma (Hingorani et al., 2005) (Figure S2A) with significant collagen deposition (visualized by picrosirius red staining, Figure S2B), macrophage (F4/80, Figure S2C) and neutrophil infiltration (MPO or S100A9, Figures S2D and S2E), few $CD3^+$ T cells (Feig et al., 2013) (Figure S2F), numerous

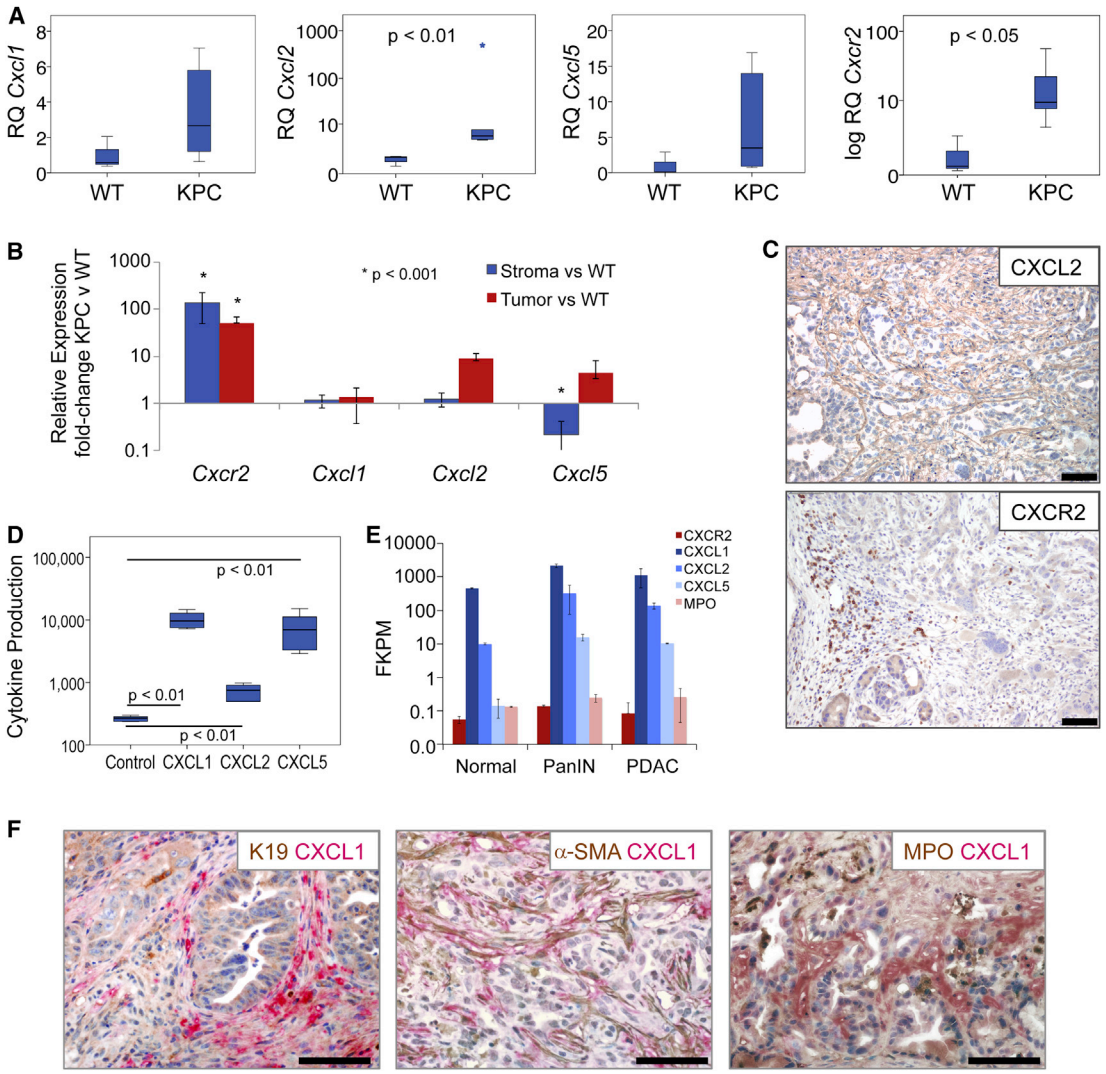

Figure 2. KPC Mice Recapitulate the Microenvironment and CXCR2 Expression of Human PDAC

(A) Expression of *Cxcr2* and its ligands in KPC PDAC (n = 6) compared with normal WT pancreas. p Values, Mann-Whitney U test.

(B) Expression of *Cxcl1, Cxcl2, Cxcl5*, and *Cxcr2* from pooled (n = 3) laser-capture micro-dissected stroma or tumor epithelium compared with WT pancreas. Expression normalized to *Gapdh*. p Value, ANOVA. Error bars are ±SEM.

(C) Representative IHC for CXCL2 and CXCR2 in PDAC from KPC mice. Scale bars represent 200 μm.

(D) Cytokine array analysis of CXCR2 ligands produced by KPC cell lines compared with control pancreatic duct epithelial cells (n = 6). p Values, Mann-Whitney U test.

(E) RNA-seq expression of *Cxc1, Cxcl2, Cxcl5*, *Cxcr2*, and *Mpo* in FAP$^+$ fibroblasts from normal pancreas, PanIN, or PDAC from KPC mice (n = 2). Error bars are ±SD.

(F) Dual IHC for CXCL1 (red) and CK19, α-SMA, or MPO (brown) in KPC tumors. See also Figure S2.

activated α-smooth muscle actin (α-SMA)-positive stellate cells (Figure S2G), abundant levels of the pro-invasive protein tenascin C (Oskarsson et al., 2011) (Figure S2H), and high levels of tumor cell proliferation (marked by Ki67, Figure S2I).

It has been previously shown that KPC tumor cells express the ligands CXCL1 and CXCL2 (Stromnes et al., 2014). When we examined the expression of CXCR2 and its ligands in tumors from KPC mice we found that, similar to human tumors, *Cxcl2* and *Cxcr2* were significantly upregulated in PDAC compared with normal pancreas, while there was also increased expression of *Cxcl1* and *Cxcl5* in a proportion of the tumors (Figure 2A). To determine the source of ligand production we performed qPCR on RNA prepared from laser-capture micro-dissected tumor epithelium and stroma. *Cxcl1*, *Cxcl2*, *Cxcl5*, and *Cxcr2* transcripts were quantified in these samples relative to wild-type (WT) pancreas. This demonstrated increased expression of *Cxcl2* and *Cxcl5* by tumor cells (Figure 2B). Similar to human tumors, *Cxcr2* was highly expressed by stromal cells, likely neutrophils, and some tumor cells (Figure 2B), and this was confirmed by IHC (Figure 2C). Indeed, previously published work has shown that there is significant infiltration of granulocytes into KPC tumors (Clark et al.,

2007), and these are likely the CXCR2-expressing cells that we observe. In addition, we found that KPC tumor cells in culture secreted substantial amounts of CXCL1 and CXCL5, and smaller amounts of CXCL2 (Figure 2D). Finally we analyzed expression of *Cxcl1*, *Cxcl2*, *Cxcl5*, and *Cxcr2* by RNA sequencing (RNA-seq) of FAP$^+$ fibroblasts isolated from normal pancreas, PanIN, and PDAC from KPC mice (Feig et al., 2013). Expression of *Cxcl1*, *Cxcl2*, and *Cxcl5* was increased in FAP$^+$ fibroblasts from PanIN and PDAC compared with WT (Figure 2E). CXCL1 expression by stromal fibroblasts was confirmed by co-IHC for CXCL1 and α-SMA (Figure 2F). CXCR2 was expressed at negligible levels in FAP$^+$ fibroblasts, and, compared with normal controls, was unchanged in PanIN and PDAC (Figure 2E). The expression we did observe was likely due to contamination by a very small number of neutrophils, given that we observe similar levels of MPO (Figure 2E). Our results show that KPC mice recapitulate the microenvironment and upregulated CXCR2 signaling seen in human PDAC, and represent an ideal model in which to investigate the role of CXCR2 signaling in pancreatic cancer.

Cxcr2 Deletion Abrogates Metastasis in KPC Mice

We generated KPC *Cxcr2*$^{-/-}$ mice, which were born at the expected Mendelian ratios and exhibited normal pancreatic pathology. There was no difference in overall or tumor-free survival between KPC *Cxcr2*$^{-/-}$ and KPC mice (Figure 3A), which initially suggested that CXCR2 was neither tumor suppressive nor tumor promoting in this system. To investigate whether inhibition of CXCR2 signaling might affect response to chemotherapy in pancreatic cancer, we treated mice with gemcitabine from 10 weeks of age. At this time mice have widespread advanced pancreatic neoplasia (Hingorani et al., 2005; Morton et al., 2010), and are more likely to mimic non-metastatic surgically resectable disease. Using this timepoint also allowed us to monitor effects of drugs or combinations over a longer period of time. This was crucial given recent studies that have generated contrasting results depending on the timing of intervention (Olive et al., 2009; Rhim et al., 2014). However, it is important to note that pancreata at this stage will exhibit mostly pre-invasive disease with occasional progression. Nevertheless, we did not detect any significant impact of gemcitabine treatment on survival in either KPC or KPC *Cxcr2*$^{-/-}$ mice (Figure 3A).

There were no clear histological differences between tumors in KPC and KPC *Cxcr2*$^{-/-}$ mice; however, we found that *Cxcr2* deletion was sufficient to almost completely abrogate metastasis (Figures 3B–3F). Unsurprisingly, gemcitabine had no significant effect on metastases in the KPC model (Figure 3B). IHC of immune cell infiltrate in pancreatic tumors from KPC and treated and untreated KPC *Cxcr2*$^{-/-}$ mice showed that, as expected, given the role of CXCR2 in neutrophil homing, there was a significant reduction in the number of MPO$^+$ cells infiltrating tumors lacking CXCR2 (Figures 3G, 3H, and S3A). Interestingly, this was accompanied by a significant increase in F4/80$^+$ macrophages and CD3$^+$ T cells in the KPC *Cxcr2*$^{-/-}$ tumors (Figures 3G, 3H, S3B, and S3C), and a significant decrease in expression of the pro-invasive protein tenascin C (Figures 3G, 3H, and S3D). There were also fewer proliferative cells in the KPC *Cxcr2*$^{-/-}$ tumors, but no difference in the levels of apoptosis, as assessed by cleaved caspase 3 IHC (Figures S3E and S3F). We also found a decrease in picrosirius red staining indicating a reduction in collagen I expression (Figure S3G).

Recently, we performed integrated genomic analysis of 456 human PDAC that defined four subtypes of PC that are associated with distinct histopathological characteristics and differential survival (Bailey et al., 2016). Based on a number of key molecular characteristics, these subtypes have been named: (1) squamous; (2) pancreatic progenitor; (3) immunogenic; and (4) aberrantly differentiated endocrine exocrine (ADEX). The squamous subtype is an independent prognostic factor and is associated with poor outcomes. To further investigate the role of CXCR2 in PDAC progression we set out to assess whether loss of CXCR2 was significantly associated with a specific PDAC subtype. This analysis clearly demonstrated that CXCR2 loss is associated with an apparent switch from the poorly prognostic squamous identity commonly observed in KPC tumors, and an enrichment of gene expression that defines the pancreatic progenitor, immunogenic, and ADEX subtypes (Figures 3I and 3J). These data are in line with our finding that *Cxcr2* deletion inhibits metastasis, and provide further evidence of a role for CXCR2 signaling in promoting aggressive pancreatic cancer.

Depletion of Ly6G+ Cells Recapitulates the Effects of *Cxcr2* Deletion

Ly6G$^+$ cells, including neutrophils and MDSCs, are the most prominent source of CXCR2 in mice (Cacalano et al., 1994). Thus, we considered whether depletion of these cells would recapitulate the phenotypes that arise as a consequence of *Cxcr2* deletion. The anti-Ly6G antibody 1A8, has been routinely used to deplete Ly6G$^+$ cells, and is well-tolerated and effective long term (Jamieson et al., 2012). KPC mice were treated from 10 weeks of age with 1A8 or 2A3 isotype control. Compared with 2A3-treated mice, and like *Cxcr2* deletion, 1A8 treatment had no effect on survival (Figure 4A), but did result in strong suppression of metastasis (Figure 4B), indicating that the CXCR2-dependent recruitment of Ly6G$^+$ cells is indeed important in the establishment of secondary disease. As expected, the primary tumors of 1A8-treated mice contained fewer MPO$^+$ neutrophils than tumors from 2A3-treated mice and, importantly, 1A8$^+$ cells were also reduced even at endpoint in both tumor and spleen (Figures 4C–4F), suggesting that treatment remains effective even if some antibody neutralization may occur. F4/80$^+$ macrophage infiltration did not change, but, like *Cxcr2* deletion, the depletion of Ly6G$^+$ cells resulted in a marked increase in the number of infiltrating CD3$^+$ T cells (Figures 4C–4E), supporting previous work (Stromnes et al., 2014). Thus, depletion of Ly6G$^+$ cells, the dominant cell type expressing CXCR2, has a similar effect to *Cxcr2* deletion, namely inhibition of metastasis, and substantial changes in the immune cell profile of tumors, most notably a loss of MPO$^+$ neutrophils and a marked increase in CD3$^+$ T cells.

Although these data suggest that Ly6G$^+$ cells mediate the effects of *Cxcr2* deletion, others have reported a pro-tumorigenic role for CXCR2 signaling in pancreatic tumor cells (Purohit et al., 2016; Wang et al., 2013). To confirm that the effects of *Cxcr2* deletion were not mediated by effects on autocrine tumor cell signaling we deleted *Cxcr2* specifically from the pancreatic epithelium of KPC mice using a conditional floxed *Cxcr2* allele

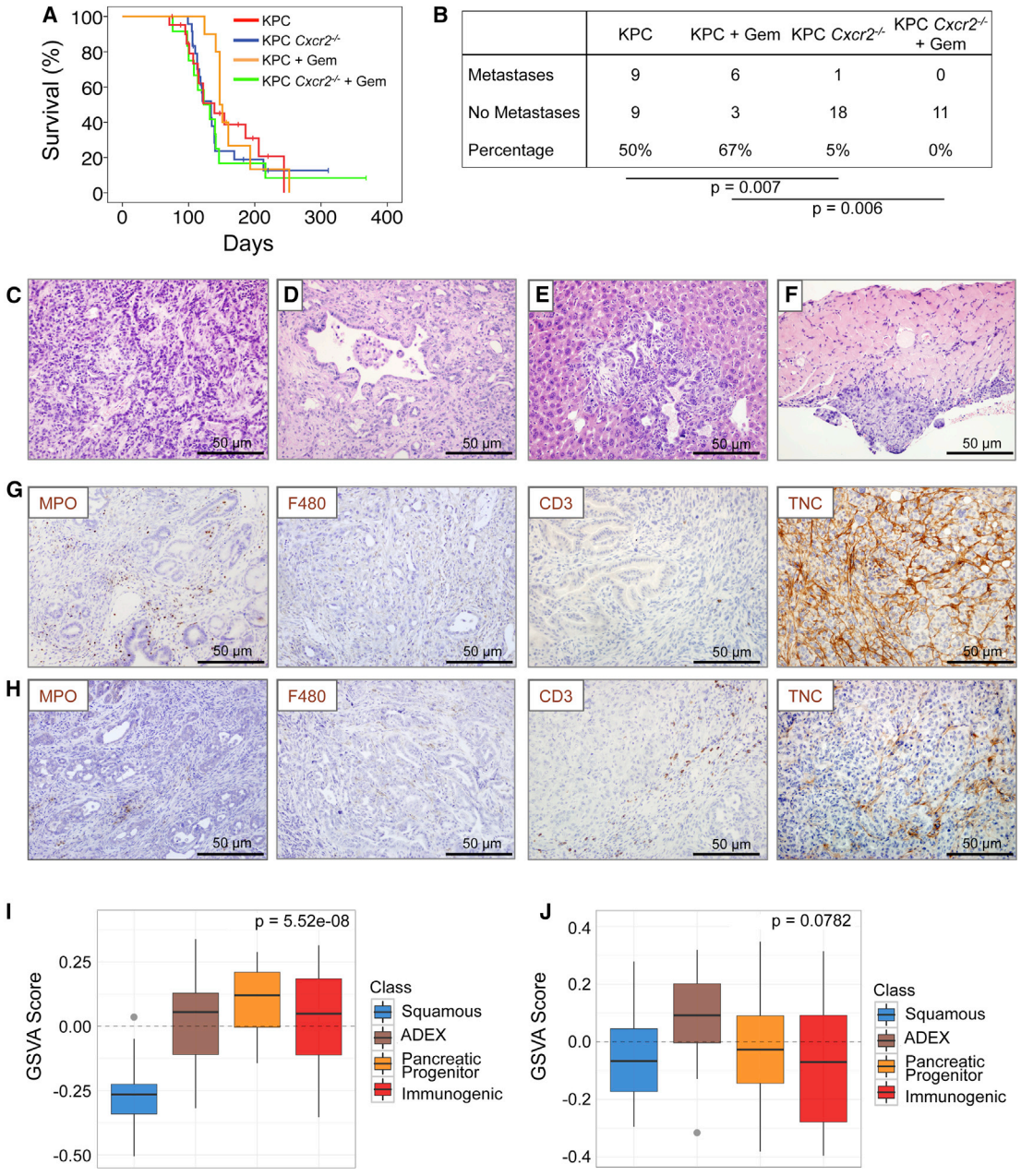

Figure 3. *Cxcr2* Deletion Inhibits Metastasis in KPC Mice

(A) Kaplan-Meier survival analysis of KPC and KPC *Cxcr2*$^{-/-}$ mice untreated, or treated from 10 weeks of age with 100 mg/kg gemcitabine, n = 21, 24, 10, 13, respectively (not significant, log rank test).

(B) Table comparing incidence of metastases in KPC and KPC *Cxcr2*$^{-/-}$ mice treated as indicated. p Values, chi-square test.

(C and D) H&E staining of representative primary tumors from (C) KPC and (D) KPC *Cxcr2*$^{-/-}$ mice.

(E and F) H&E staining of representative (E) liver and (F) diaphragm metastasis from KPC mice.

(G and H) IHC for MPO, F4/80, CD3, and tenascin C (TNC) in tumors from (G) KPC and (H) KPC *Cxcr2*$^{-/-}$ mice.

(I and J) Boxplots of signature scores (I) upregulated and (J) downregulated, in KPC *Cxcr2*$^{-/-}$ mice, stratified by human PDAC class. p Values, Kruskall-Wallis test.

See also Figure S3.

(KPC *Cxcr2*$^{fl/fl}$). Importantly, we did not see any effect on survival (Figure 4G), and we no longer observed any effects on metastasis or CD3^{+} T cell infiltration (Figures 4H and 4I), confirming that the effects of *Cxcr2* deletion are not dependent on the loss of expression on the tumor cells.

CXCR2 Inhibition Reduces Metastases and Prolongs Survival in KPC Mice

Although anti-metastatic therapies may not inhibit growth of the primary tumor, they may be useful in patients where the primary tumor can be resected. Thus, we wanted to determine if

pharmacological inhibition of CXCR2 signaling could inhibit metastasis in the KPC model. To inhibit CXCR2, we first used a short peptide CXCR2 "pepducin" (1/2i-pal), which inhibits CXCR2 signaling by interfering with its ability to couple to intracellular signal-transduction molecules (Jamieson et al., 2012; Kaneider et al., 2005). Control mice received a scrambled pepducin. Other groups of KPC mice received gemcitabine alone, or gemcitabine along with the CXCR2 pepducin. All treatments were started when the mice were 10 weeks old. CXCR2 pepducin treatment resulted in a significant increase in survival compared with controls and appeared to reduce metastasis (Figures 5A and 5B). Gemcitabine alone had no effect on survival or the development of metastasis, but when CXCR2 pepducin and gemcitabine were combined, survival was significantly extended and we were unable to detect any metastases in these animals (Figures 5A and 5B). We did not see significant changes in neutrophil, macrophage, or CD3 infiltration in pepducin-treated mice (Figures 5C, 5D, and S4A–S4C), although the number of infiltrating neutrophils was significantly higher in mice treated with the combination of CXCR2 pepducin and gemcitabine (Figure S4A), which may be due in part to necrosis within these tumors. Indeed, tenascin C, the expression of which is induced by hypoxia (Lal et al., 2001), was upregulated in pepducin-treated tumors (Figures 5C, 5D, and S4D). There was no significant change in either tumor cell proliferation or apoptosis (Figures S4E and S4F), but again we saw a decrease in picrosirius red staining indicating a reduction in collagen I (Figure S4G).

CXCR2 Inhibition Results in Failure to Set up a Metastatic Niche

Given the profound effect that inhibiting CXCR2 signaling has on metastasis in our model, we sought to examine potential mechanisms for this phenomenon, particularly in distant metastatic sites. MDSCs are immature bone marrow cells typified by the expression of CD11b, Gr1, and Ly6G/Ly6C (Youn and Gabrilovich, 2010). They have been shown to play a role in establishing the metastatic niche in different metastatic tumor models (Acharyya et al., 2012; Yan et al., 2010). Therefore, we investigated the levels of these, and other immune cells, in the pre-metastatic livers of KPC mice (Figure S4H), in KPC liver metastases (Figure S4I), in the livers of KPC mice treated with pepducin and gemcitabine from 10 weeks old (Figure S4J), and in liver metastases from KPC mice treated with CXCR2 pepducin and gemcitabine when symptomatic (Figure S4K). We included this latter group because of the lack of metastases in KPC *Cxcr2*$^{-/-}$ mice and mice with CXCR2 inhibited from 10 weeks.

We found that there were a substantial number of F4/80^{+} macrophages, NIMP1^{+} neutrophils, and cells staining positively with the MDSC marker, S100A9, in the pre-metastatic liver (Figure S4H), and in established liver metastases where there were also CXCR2-expressing cells (Figure S4I). CXCR2 inhibition with pepducin considerably decreased the number of myeloid cells in the livers of KPC mice (Figure S4J) and, even in mice with late-stage tumors, reduced the number of neutrophils and S100A9^{+} cells infiltrating liver metastases, although had no effect on monocyte/macrophage recruitment (Figure S4K). Interestingly, the number of CD3^{+} T cells infiltrating these metastases was increased compared with untreated mice, in line with our observations in primary tumors. The changes we observe in primary tumors and metastases following CXCR2 inhibition suggest that the migration of myeloid lineage cells to the tumor microenvironment is impaired when CXCR2 signaling is suppressed. This reduction in chemotaxis may also result in a failure of myeloid cells to migrate to the liver and establish a niche for tumor cells. These findings suggest a key role for CXCR2 signaling and immune cell migration in metastatic progression in this model.

Clinically Relevant Targeting of CXCR2 Reduces Metastases and Prolongs Survival in KPC Mice

The finding that CXCR2 inhibition but not constitutive knockout could slow tumorigenesis suggested that CXCR2 might play opposing roles in early and late tumorigenesis. Loss during initiation might allow pre-neoplastic PanIN lesions to progress beyond senescence, while loss at late stages might inhibit the growth and metastatic potential of PDAC. Thus, we wanted to further test the therapeutic effects of CXCR2 inhibition at a later stage of neoplasia, using a clinically relevant CXCR2 inhibitor. Therefore, we tested the effects of AZ13381758, a small-molecule inhibitor of CXCR2 (referred to as CXCR2 SM) that is related to AZD5069 (Nicholls et al., 2015). AZ13381758 is a potent inhibitor of both murine and human CXCR2 (Figures S5A–S5F, Table S1), the efficacy of which was confirmed by full blood-count analysis showing increased circulating neutrophils due to their inability to home (Figure 6A).

Similar to CXCR2 pepducin, treatment with CXCR2 SM alone from 10 weeks of age prolonged the survival of KPC mice, and was most effective in combination with gemcitabine (Figure 6B). In addition, mice treated with CXCR2 SM were significantly protected from metastasis (Figure 6C). We did not observe significant changes in the number of intra-tumoral neutrophils or macrophages (Figures 6D, 6F, S5G, and S5H), similar to pepducin treatment; however, we did observe an increase in infiltrating T cells (Figures 6D, 6F, and S5I), similar to the results seen in KPC *Cxcr2*$^{-/-}$ mice. We also saw a reduction of tenascin C (Figures 6D, 6F, and S5J), a reduction in the number of proliferative cells (Figure S5K), no change in apoptosis (Figure S5L), and a reduction in stromal collagen (Figure S5M) in CXCR2 SM-treated tumors. Thus, like *Cxcr2* deletion or Ly6G^{+} cell depletion, pharmacological inhibitors of CXCR2 can reduce the metastatic spread of pancreatic tumors in KPC mice and may provide a survival advantage over control animals. More significantly, the combination of CXCR2 inhibition and gemcitabine treatment extends the life span of KPC mice by 50–70 days and substantially suppresses metastasis.

CXCR2 Inhibition Substantially Enhances Sensitivity to Anti-PD1 Immunotherapy

There is a growing awareness that immunosuppression by infiltrating immune cells plays an important role in the resistance of tumors to endogenous anti-tumor immune responses as well as therapeutic interventions. Pancreatic cancer cells themselves actively contribute to immune suppression through production of cytokines (Beatty et al., 2011), so that although a systemic anti-tumor immune response is elicited, it is ineffective (Dodson et al., 2011). The efficacy of therapy in PDAC would likely be improved by overcoming this immune suppression. Indeed, immunotherapy aimed at harnessing endogenous

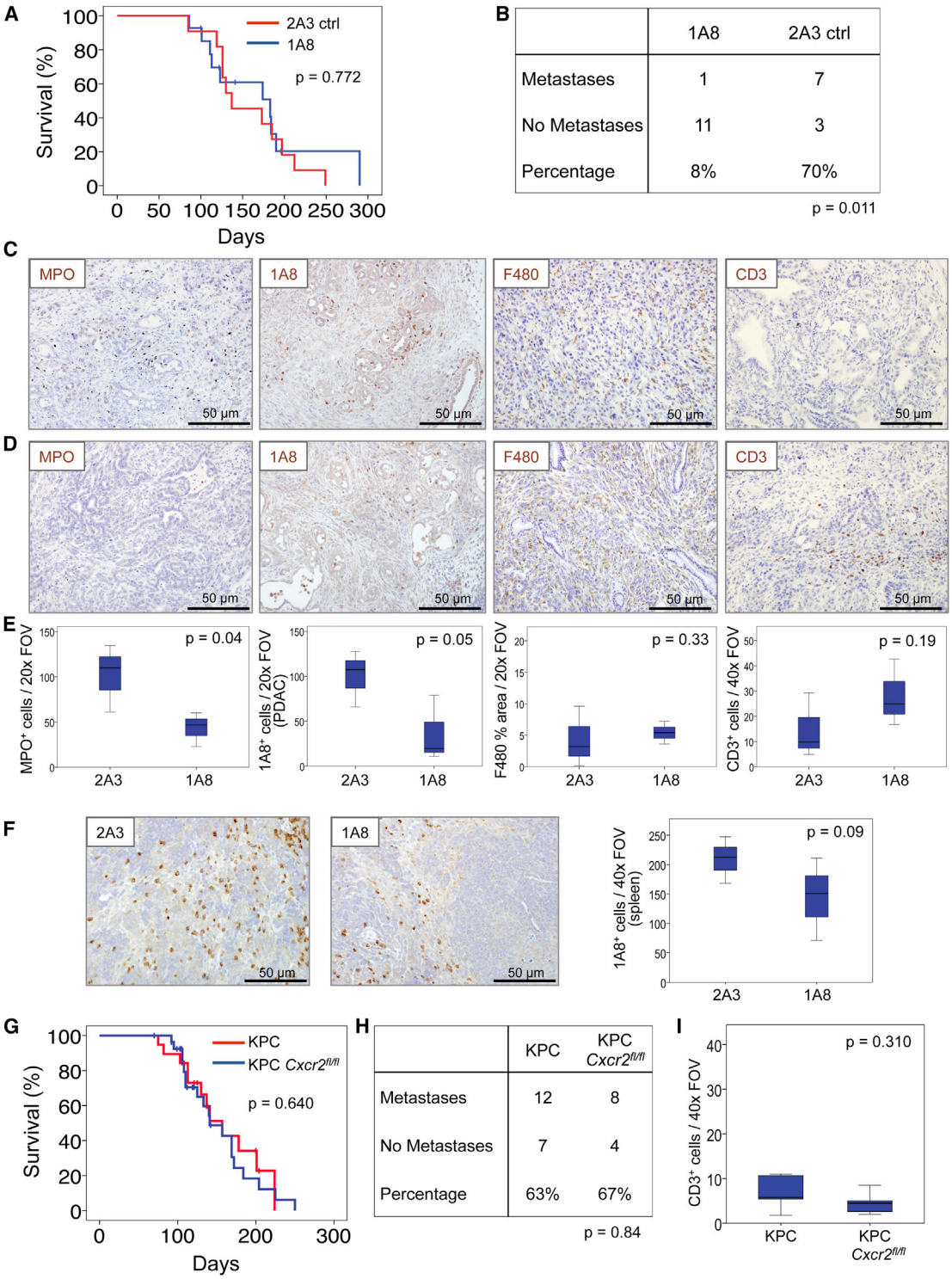

Figure 4. Neutrophil Ablation Also Inhibits Metastasis in the KPC Model

(A) Kaplan-Meier analysis of survival of KPC mice treated from 10 weeks of age with 2A3 isotype-control antibody (n = 11) or 1A8, anti-Ly6G neutrophil-ablating antibody (n = 15). p Values, log rank test.

(B) Table comparing incidence of metastases in KPC mice treated with 2A3 or 1A8. p Value, chi-square test.

(C and D) IHC on tumors from (C) 2A3- or (D) 1A8-treated mice, for MPO, 1A8, F480, and CD3.

(E) Boxplots showing quantification of IHC in (C) and (D). p Values, Mann-Whitney U test.

(legend continued on next page)

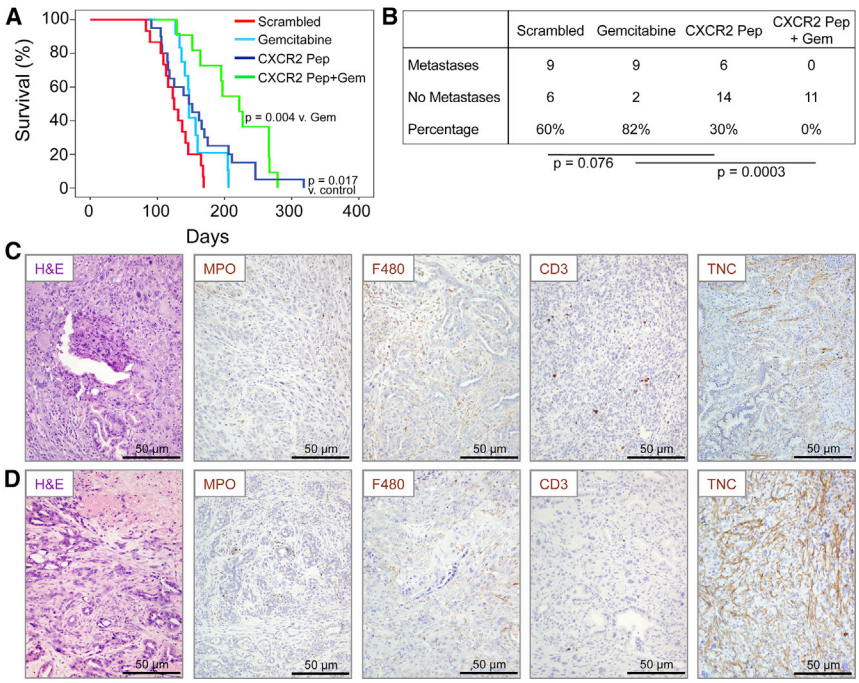

Figure 5. *Cxcr2* Inhibition Inhibits Metastasis and Prolongs Survival in KPC Mice

(A) Kaplan-Meier analysis of KPC mice treated from 10 weeks of age with scrambled pepducin (n = 15), gemcitabine (n = 14), CXCR2-inhibiting pepducin (n = 20), or CXCR2-inhibiting pepducin + gemcitabine (n = 11). p Values, log rank test.

(B) Table comparing incidence of metastases in KPC mice treated as indicated. p Values, chi-square test.

(C and D) H&E staining and IHC for MPO, F4/80, CD3, and tenascin C (TNC) in tumors in response to (C) scrambled pepducin and (D) CXCR2-targeting pepducin. See also Figure S4.

anti-tumor immunity has shown promise in multiple tumor types (Sharma and Allison, 2015). Given that *Cxcr2* deletion or inhibition increased the number of $CD3^+$ T cells in pancreatic tumors in KPC mice, we wanted to know if CXCR2 inhibitors could enhance sensitivity to therapies aimed at de-repressing T cells. We chose to use anti-PD1 antibodies, which block T cell suppression by preventing interactions between PD1 and its ligands (Barber et al., 2006; Fife et al., 2009), but which have previously been found to be ineffective as a single agent in this model (Winograd et al., 2015).

In this experiment, treatment was only started once the KPC mice had developed palpable pancreatic tumors. One group of mice then received CXCR2 SM for 2 weeks to increase T cell infiltration into the tumor. Control mice received either vehicle alone or gemcitabine alone. After this initial priming phase, animals in the CXCR2 SM and vehicle groups received anti-PD1 antibody while continuing on the CXCR2 SM or vehicle treatments. Unsurprisingly, given that they are carrying late-stage tumors, few vehicle-treated animals survived long enough (2 weeks) to allow commencement of PD1 treatment (Figure 7A). Remarkably, however, even in these late-stage tumors, treatment with CXCR2 SM and anti-PD1 significantly extended survival beyond that of the mice treated with vehicle plus anti-PD1, with two mice living 100 days beyond the start of treatment before succumbing to pancreatic tumors (Figure 7A).

When tumors from mice at endpoint were examined by IHC for Ki67 and cleaved caspase 3 (CC3) we observed a reduction in proliferation following CXCR2 SM + anti-PD1 treatment (Figures 7B and 7C), but no change in apoptosis (Figures 7D and 7E), although both tumor cells and cells of the microenvironment may contribute to this phenotype. Analysis of the tumors by flow cytometry confirmed the presence of an increased percentage of $CD3^+$ T cells in CXCR2 SM + anti-PD1-treated tumors following 2 weeks of treatment (Figure 7F). We were able to show by both IHC (Figure 7G) and fluorescence-activated cell sorting (FACS) analysis (Figure 7H) that the number of both $CD4^+$ and $CD8^+$ T cells was increased in CXCR2 SM-treated mice and, importantly, the number of inhibitory regulatory T cells was actually reduced (Figure 7H). Interestingly, in vehicle-treated mice a substantial proportion of both $CD4^+$ and $CD8^+$ T cells exhibited an effector memory phenotype ($CD62L^-CD44^+$). In contrast, in CXCR2 SM-treated mice, this population was less abundant, and a greater proportion of the $CD4^+$ and $CD8^+$ T cells expressed a naive T cell phenotype ($CD62L^+CD44^-$) perhaps allowing for increased intratumoral T cell priming (Figure 7I).

Collectively, our data show that in KPC mice, *Cxcr2* deficiency, $Ly6G^+$ cell depletion, or pharmacological inhibition of CXCR2 suppresses metastasis in PDAC, and that CXCR2 inhibitors enhance response to chemotherapeutics and immunotherapy to prolong survival. These results suggest that CXCR2 targeting might have therapeutic efficacy in the pre-metastatic setting, and may provide an opportunity for immunotherapy in pancreatic cancer.

DISCUSSION

The outcome for patients suffering from PDAC remains dismal (Siegel et al., 2015), and it is clear that improvements in pancreatic cancer treatment are required. Here, we show that CXCR2 signaling in the myeloid compartment is tumor promoting and required for pancreatic cancer metastasis, and in the notoriously therapy-resistant KPC model of pancreatic cancer we highlight therapeutic opportunities: Not only does inhibition of CXCR2

(F) IHC for 1A8 on spleens from 2A3- and 1A8-treated mice, quantified on right. p Values, Mann-Whitney U test.

(G) Kaplan-Meier survival analysis of KPC (n = 19, median = 157 days) and KPC $Cxcr2^{fl/fl}$ mice (n = 28, median = 141 days). p Values, log rank test.

(H) Table comparing incidence of metastases in KPC and KPC $Cxcr2^{fl/fl}$ mice. p Values, chi-square test.

(I) Boxplots showing quantification of CD3 IHC in tumors from KPC and KPC $Cxcr2^{fl/fl}$ mice. p Value, Mann-Whitney U test.

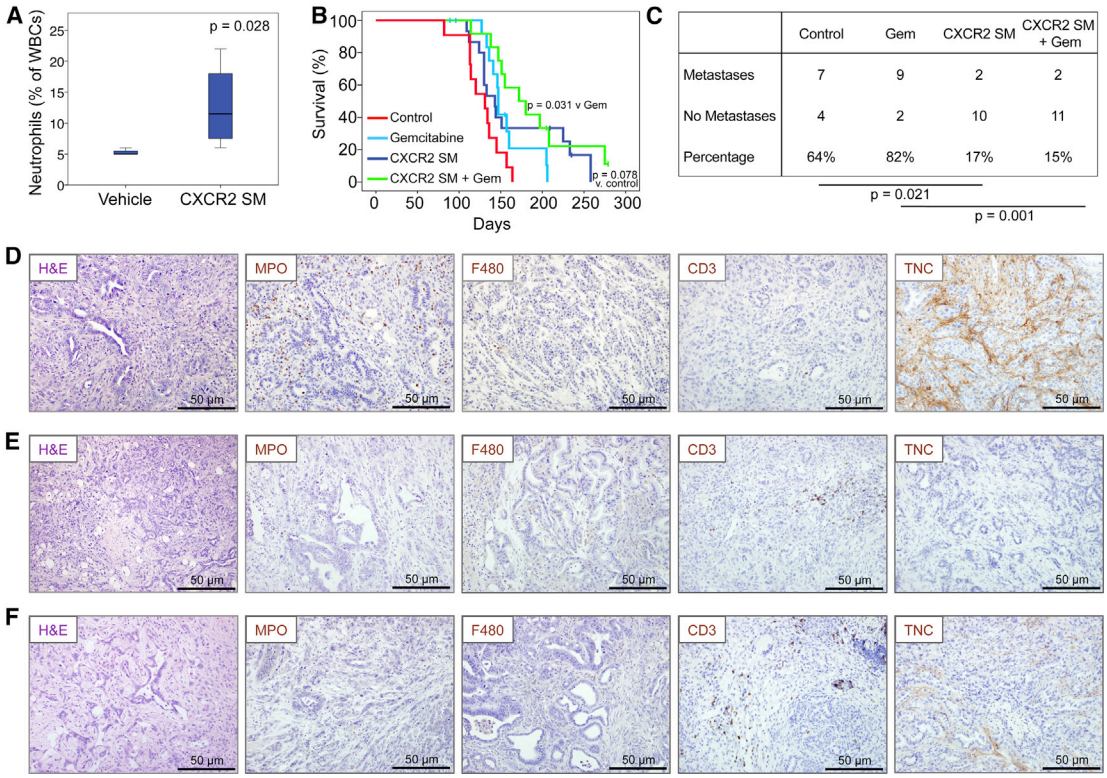

Figure 6. Therapeutic Targeting of CXCR2 Inhibits Metastasis and Prolongs Survival in KPC Mice

(A) Boxplot showing circulating neutrophils in CXCR2 SM-treated mice (n = 4). p Values, Mann-Whitney U test.

(B) Kaplan-Meier survival analysis of KPC mice treated from 10 weeks of age with vehicle (n = 11), gemcitabine (n = 14), CXCR2 SM (n = 15), or CXCR2 SM + gemcitabine (n = 12). p Values, log rank test.

(C) Table comparing incidence of metastases in KPC mice treated as indicated. p Values, chi-square test.

(D–F) H&E staining and IHC for MPO, F4/80, CD3, and tenascin C (TNC) in tumors in response to (D) vehicle, (E) CXCR2 SM, and (F) CXCR2 SM + gemcitabine. See also Figure S5 and Table S1.

prevent metastasis; it also augments the efficacy of immune checkpoint inhibitors by allowing T cell infiltration. Indeed, when we compare our mouse tumors with human tumors, we find that *Cxcr2* deletion is associated with a switch away from the poorly prognostic squamous identity (Bailey et al., 2016).

Our data support other studies linking inflammation and metastasis (Colotta et al., 2009; Kim et al., 2009) and suggest that inflammatory signaling molecules may be excellent targets in the neoadjuvant treatment of pancreatic cancer. A number of key inflammatory pathways, including IL-6/STAT3, NF-κB, and COX2 pathways, have already been shown to be key in the process of PDAC progression and metastasis (Corcoran et al., 2011; Daniluk et al., 2012; Fukuda et al., 2011; Lesina et al., 2011; Ling et al., 2012). Indeed, patients with significant tumor-associated inflammation have a poor prognosis following surgery (Jamieson et al., 2005).

It has been suggested that pancreatic tumors metastasize prior to the development of a detectable mass in the pancreas (Haeno et al., 2012; Rhim et al., 2012). However, we found that whether CXCR2 signaling was targeted by genetic or pharmacological means, alone, or in combination with chemotherapy, metastasis was significantly inhibited. The ameliorated recruitment of immature myeloid cells to metastatic sites suggests that CXCR2 functions at multiple stages of the metastatic process, hence the striking effect on metastases seen following genetic knockout. In addition, given that CXCR2 inhibition can restrict pancreatitis, targeting CXCR2 signaling in cancer may have additional benefit in terms of ameliorating symptoms (Steele et al., 2015).

Predicting the outcome of targeting stromal elements within PDAC has been difficult. Combination of anti-stromal agents and chemotherapy represents a promising approach to therapy in this disease, with encouraging findings in studies targeting the extracellular matrix glycosaminoglycan or hyaluronic acid (Jacobetz et al., 2013). On the other hand, recent studies targeting tumor-associated fibroblasts and hedgehog signaling at different stages of tumorigenesis produced differing results, with accelerated tumorigenesis if treatment was early and improved survival for late-stage treatment (Olive et al., 2009; Ozdemir et al., 2014; Rhim et al., 2014). The results we present here suggest that CXCR2 has stage- and also cell-type-specific roles in PDAC cancer. During early carcinogenesis, CXCR2 can reinforce senescence in epithelial cells (Acosta et al., 2008); however, once the senescence pathway is abrogated, MDSC/neutrophil CXCR2 drives tumor progression and metastasis. We propose this as the reason that *Cxcr2* deletion had no overall effect on survival of KPC mice. These findings are consistent with the expression of CXCR2 in human cancer, which is expressed in

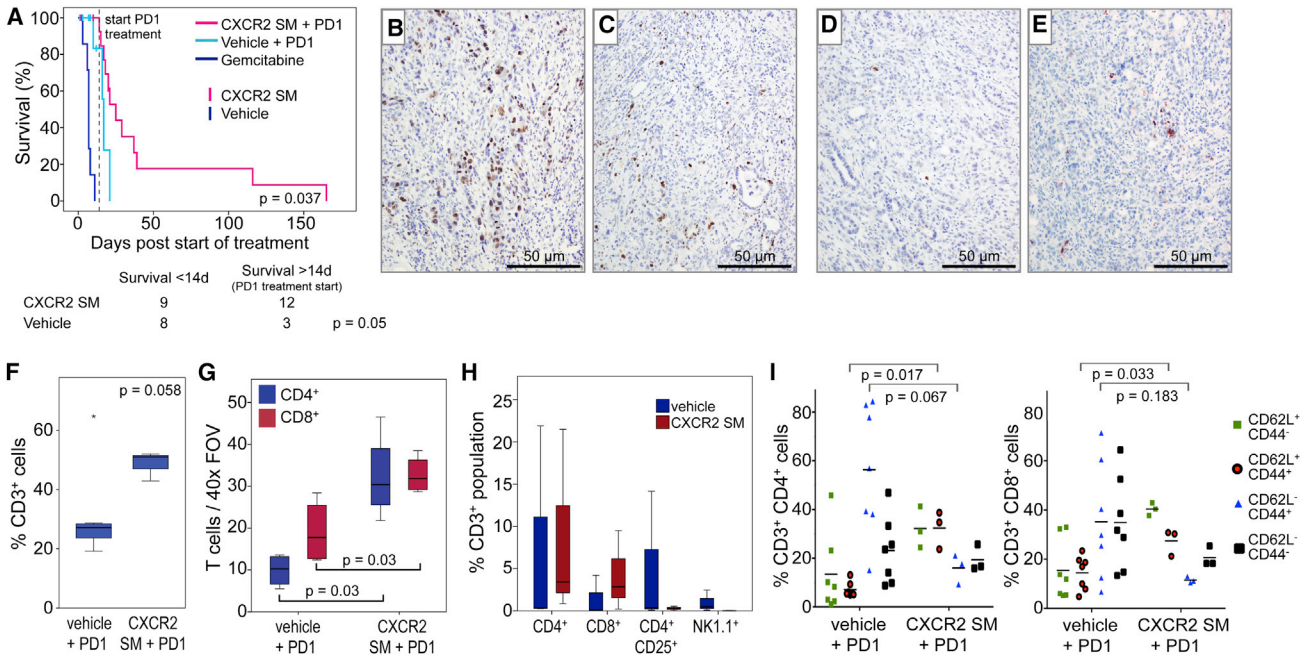

Figure 7. CXCR2 Blockade Promotes T Cell Infiltration into Tumors and Sensitivity to Immunotherapy

(A) Kaplan-Meier survival analysis of tumor-bearing KPC mice treated with either gemcitabine, CXCR2 SM alone for 2 weeks, and then in combination with anti-PD1, vehicle alone for 2 weeks, and then combined with anti-PD1, CXCR2 SM alone (censors on pink line), or vehicle alone (censors on cyan line). Few mice on vehicle alone survived for 2 weeks to allow PD1 treatment as shown in the table below. p Values, chi-square test.

(B and C) IHC for Ki67 in tumors from KPC mice treated with (B) vehicle + PD1 or (C) CXCR2 SM + PD1.

(D and E) IHC for cleaved caspase 3 in tumors from KPC mice treated with (D) vehicle + PD1 or (E) CXCR2 SM + PD1.

(F) FACS analysis of intratumoral $CD3^+$ cells in mice treated as indicated.

(G) Boxplot showing quantification of IHC for $CD4^+$ and $CD8^+$ T cells in tumors from KPC mice treated as indicated.

(H) FACS analysis of intratumoral $CD4^+$, $CD8^+$, $CD4^+CD25^+$, and $NK1.1^+$ cells (% of $CD3^+$ cells) in mice treated as indicated.

(I) FACS profile of $CD4^+$ and $CD8^+$ T cells isolated from tumors in mice treated with either vehicle + anti-PD1 or CXCR2 SM + anti-PD1. (F–I) n = 3. p Values, Mann-Whitney U test.

PanINs and more rarely in epithelial tumor cells, but is highly expressed in neutrophils/MDSCs at tumor fronts.

We do find that a subset of human tumors show high epithelial CXCR2 expression; however, it is unclear what role CXCR2 is playing in those tumors. Many studies have shown that CXCR2 expression on cancer cells can drive proliferation, invasion, and migration (Matsuo et al., 2009a, 2009b; Purohit et al., 2016; Wang et al., 2013). However, our data showing that epithelial cell-specific *Cxcr2* loss has no effect on tumor-free survival or metastasis suggests that the effects we observe in the case of *Cxcr2* deletion or inhibition are not mediated by tumor cell expression. Together, these findings highlight an intriguing idea, namely, that tumor cells develop a requirement for autocrine CXCR2 signaling once explanted, as a result of loss of the paracrine signaling that exists in vivo. This hypothesis would further underscore the importance of CXCR2 signaling in pancreatic cancer.

Given that most of the mutations that accompany *KRAS* mutation in PDAC have been shown to abrogate growth arrest/senescence, for example *CDKN2A*, *TP53*, and TGFβ pathway-targeting mutations, and the fact that at the time of presentation tumors are highly proliferative and not senescent, concerns over treatment of patients with PDAC with CXCR2 inhibitors are negated. Any remaining concerns are alleviated given the good efficacy we have seen with combination with gemcitabine or anti-PD1. This clearly differentiates CXCR2 inhibition from other stromal targeting agents such as hedgehog inhibitors.

Among the stromal changes we observed following CXCR2 inhibition, one of the most striking was enhanced T cell infiltration. This enhanced T cell infiltration may be responsible for the increased efficacy of gemcitabine, given that enhanced T cell accumulation in KPC tumors can induce stromal remodeling (Stromnes et al., 2015), which in turn can increase the efficacy of gemcitabine (Olive et al., 2009; Provenzano et al., 2012). The infiltration of T cells also rendered tumors sensitive to immunotherapy with PD1-blocking antibody. There are a number of possible mechanisms by which CXCR2 inhibition enables T cell infiltration. For example, we observed a decrease in monocyte/macrophage tumor infiltration in treated mice, and a role for macrophages in the exclusion of T cells from pancreatic tumors has been described (Beatty et al., 2015).

Immunotherapy to reactivate anti-tumor immunity has delivered promising results in several tumor types (Sharma and Allison, 2015), but not, as yet, in pancreatic cancer. Dose scheduling will be important in future clinical trials, given that CXCR2 targeting may be most effective when used to prime the tumor microenvironment. Indeed, the anti-metastatic effect we observe was uncovered when treating mice at an early time point with mostly pre-invasive disease and, as such, may not truly reflect the clinical situation. Nevertheless, our results

suggest that inhibiting CXCR2 signaling, and thus recruitment of myeloid cells, may offer the opportunity for immunotherapy in pancreatic cancer, even in patients not eligible for resection. In addition, neoadjuvant targeting of CXCR2 in combination with standard chemotherapy could provide hope for effective targeting of disease progression and metastases in resectable PDAC.

EXPERIMENTAL PROCEDURES

Human Pancreatic Cancer Tissue

All tissue was collected prospectively following informed patient consent. West of Scotland Research Ethics Committee 4 approved the study. For further information see Supplemental Experimental Procedures.

Animal Experiments

All animal experiments were performed under UK Home Office license and approved by the University of Glasgow Animal Welfare and Ethical Review Board. For further information see Supplemental Experimental Procedures.

Cytokine Array on Medium Conditioned by KPC Cells

Murine pancreatic cancer cell lines have been described previously (Morton et al., 2010). AAM-CYT-G2000-4 Ray Biotech slides (Holzel Diagnostics) were used according to the manufacturer's protocol. Laser scanning using the Cy3 channel was used for detection of protein expression.

In Vivo Treatment Experiments

For drug treatments, mice were randomly assigned to cohorts. Treatments used were: CXCR2 pepducin (X1/2pal-i3, Genscript) or scrambled pepducin at 2.5 mg/kg by subcutaneous injection daily; gemcitabine (LC Laboratories) at 100 mg/kg by intraperitoneal (i.p.) injection twice weekly; CXCR2 SM (AstraZeneca) at 100 mg/kg per os (p.o.) twice daily; vehicle p.o. twice daily; anti-PD1 (Biolegend) or isotype control at 10 mg/kg by i.p. injection twice weekly; 1A8 antibody or 2A3 isotype control (BioXcell) at 10 mg/kg by i.p. injection thrice weekly. Efficacy testing of CXCR2 SM is described in Supplemental Experimental Procedures.

Statistical Analysis

Kaplan-Meier survival analysis was performed using log rank tests. Assessment of differences in counts between different mice was performed using non-parametric Mann-Whitney U tests. For all boxplots in the paper, boxes depict the middle 50% of the records and the line indicates the median. Whiskers show the highest and lowest values that are no greater than 1.5 times the interquartile (IQ) range, and asterisks show outliers (cases with values between 1.5 and 3 times the IQ range). Chi-square tests were used to assess the statistical differences in metastasis rate between categorical groups. Spearman's rho correlation coefficient method was used to assess correlation. ANOVA test was used for analysis of qPCR data.

ACCESSION NUMBERS

RNA-seq data are available in the ArrayExpress database (www.ebi.ac.uk/arrayexpress) under accession number ArrayExpress: E-MTAB-4659.

SUPPLEMENTAL INFORMATION

Supplemental Information includes Supplemental Experimental Procedures, five figures, and one table and can be found with this article online at http://dx.doi.org/10.1016/j.ccell.2016.04.014.

AUTHOR CONTRIBUTIONS

C.W.S., study design, data acquisition, data analysis, and drafting of manuscript; S.A.K., J.D.G.L., R.U.-G., L.R., M.F., S.B., K.M., Z.W., C.E., J.B.C., M.C., C.N., J.C., N.B., D.K.C., and D.S., data acquisition and analysis; P.B., data acquisition and analysis and drafting of the manuscript; F.B., C.R.C., T.R.J.E., and A.V.B., study supervision; S.B. and R.B.J.N., study concept and design, data analysis, and drafting of manuscript; O.J.S., study concept and design, study supervision, data analysis, and drafting of manuscript; J.P.M., study concept and design, study supervision, data acquisition, data analysis, and drafting of manuscript. All authors read and agreed on the final manuscript.

ACKNOWLEDGMENTS

The authors would like to thank the Cancer Research UK Glasgow Centre and the BSU facilities and Histology Service at the Cancer Research UK Beatson Institute. We would also like to thank Jane Hair for curation of the NHSGCC Biorepository and Steve Connolly (AstraZeneca, Molndal) for providing AZ13381758. This work was funded by Cancer Research UK (C596/A18076, C596/A17196) and by a Wellcome Trust Research Training Fellowship (096021, C.W.S.).

Received: August 22, 2015
Revised: February 9, 2016
Accepted: April 29, 2016
Published: June 2, 2016

REFERENCES

Acharyya, S., Oskarsson, T., Vanharanta, S., Malladi, S., Kim, J., Morris, P.G., Manova-Todorova, K., Leversha, M., Hogg, N., Seshan, V.E., et al. (2012). A CXCL1 paracrine network links cancer chemoresistance and metastasis. Cell *150*, 165–178.

Acosta, J.C., O'Loghlen, A., Banito, A., Guijarro, M.V., Augert, A., Raguz, S., Fumagalli, M., Da Costa, M., Brown, C., Popov, N., et al. (2008). Chemokine signaling via the CXCR2 receptor reinforces senescence. Cell *133*, 1006–1018.

Almoguera, C., Shibata, D., Forrester, K., Martin, J., Arnheim, N., and Perucho, M. (1988). Most human carcinomas of the exocrine pancreas contain mutant c-K-ras genes. Cell *53*, 549–554.

Bailey, P., Chang, D.K., Nones, K., Johns, A.L., Patch, A.M., Gingras, M.C., Miller, D.K., Christ, A.N., Bruxner, T.J., Quinn, M.C., et al. (2016). Genomic analyses identify molecular subtypes of pancreatic cancer. Nature *531*, 47–52.

Barber, D.L., Wherry, E.J., Masopust, D., Zhu, B., Allison, J.P., Sharpe, A.H., Freeman, G.J., and Ahmed, R. (2006). Restoring function in exhausted CD8 T cells during chronic viral infection. Nature *439*, 682–687.

Baumgart, S., Ellenrieder, V., and Fernandez-Zapico, M.E. (2013). Oncogenic transcription factors: cornerstones of inflammation-linked pancreatic carcinogenesis. Gut *62*, 310–316.

Baumgart, S., Chen, N.M., Siveke, J.T., Konig, A., Zhang, J.S., Singh, S.K., Wolf, E., Bartkuhn, M., Esposito, I., Hessmann, E., et al. (2014). Inflammation-induced NFATc1-STAT3 transcription complex promotes pancreatic cancer initiation by KrasG12D. Cancer Discov. *4*, 688–701.

Bayne, L.J., Beatty, G.L., Jhala, N., Clark, C.E., Rhim, A.D., Stanger, B.Z., and Vonderheide, R.H. (2012). Tumor-derived granulocyte-macrophage colony-stimulating factor regulates myeloid inflammation and T cell immunity in pancreatic cancer. Cancer Cell *21*, 822–835.

Beatty, G.L., Chiorean, E.G., Fishman, M.P., Saboury, B., Teitelbaum, U.R., Sun, W., Huhn, R.D., Song, W., Li, D., Sharp, L.L., et al. (2011). CD40 agonists alter tumor stroma and show efficacy against pancreatic carcinoma in mice and humans. Science *331*, 1612–1616.

Beatty, G.L., Winograd, R., Evans, R.A., Long, K.B., Luque, S.L., Lee, J.W., Clendenin, C., Gladney, W.L., Knoblock, D.M., Guirnalda, P.D., and Vonderheide, R.H. (2015). Exclusion of T Cells from pancreatic carcinomas in mice is regulated by Ly6C F4/80 extra-tumor macrophages. Gastroenterology *149*, 201–210.

Burris, H.A., 3rd, Moore, M.J., Andersen, J., Green, M.R., Rothenberg, M.L., Modiano, M.R., Cripps, M.C., Portenoy, R.K., Storniolo, A.M., Tarassoff, P., et al. (1997). Improvements in survival and clinical benefit with gemcitabine as first-line therapy for patients with advanced pancreas cancer: a randomized trial. J. Clin. Oncol. *15*, 2403–2413.

Cacalano, G., Lee, J., Kikly, K., Ryan, A.M., Pitts-Meek, S., Hultgren, B., Wood, W.I., and Moore, M.W. (1994). Neutrophil and B cell expansion in mice that lack the murine IL-8 receptor homolog. Science *265*, 682–684.

Clark, C.E., Hingorani, S.R., Mick, R., Combs, C., Tuveson, D.A., and Vonderheide, R.H. (2007). Dynamics of the immune reaction to pancreatic cancer from inception to invasion. Cancer Res. *67*, 9518–9527.

Colotta, F., Allavena, P., Sica, A., Garlanda, C., and Mantovani, A. (2009). Cancer-related inflammation, the seventh hallmark of cancer: links to genetic instability. Carcinogenesis *30*, 1073–1081.

Conroy, T., Desseigne, F., Ychou, M., Bouche, O., Guimbaud, R., Becouarn, Y., Adenis, A., Raoul, J.L., Gourgou-Bourgade, S., de la Fouchardiere, C., et al. (2011). FOLFIRINOX versus gemcitabine for metastatic pancreatic cancer. N. Engl. J. Med. *364*, 1817–1825.

Corcoran, R.B., Contino, G., Deshpande, V., Tzatsos, A., Conrad, C., Benes, C.H., Levy, D.E., Settleman, J., Engelman, J.A., and Bardeesy, N. (2011). STAT3 plays a critical role in KRAS-induced pancreatic tumorigenesis. Cancer Res. *71*, 5020–5029.

Daniluk, J., Liu, Y., Deng, D., Chu, J., Huang, H., Gaiser, S., Cruz-Monserrate, Z., Wang, H., Ji, B., and Logsdon, C.D. (2012). An NF-kappaB pathway-mediated positive feedback loop amplifies Ras activity to pathological levels in mice. J. Clin. Invest. *122*, 1519–1528.

Diaz-Montero, C.M., Salem, M.L., Nishimura, M.I., Garrett-Mayer, E., Cole, D.J., and Montero, A.J. (2009). Increased circulating myeloid-derived suppressor cells correlate with clinical cancer stage, metastatic tumor burden, and doxorubicin-cyclophosphamide chemotherapy. Cancer Immunol. Immunother. *58*, 49–59.

Dodson, L.F., Hawkins, W.G., and Goedegebuure, P. (2011). Potential targets for pancreatic cancer immunotherapeutics. Immunotherapy *3*, 517–537.

Eash, K.J., Greenbaum, A.M., Gopalan, P.K., and Link, D.C. (2010). CXCR2 and CXCR4 antagonistically regulate neutrophil trafficking from murine bone marrow. J. Clin. Invest. *120*, 2423–2431.

Feig, C., Jones, J.O., Kraman, M., Wells, R.J., Deonarine, A., Chan, D.S., Connell, C.M., Roberts, E.W., Zhao, Q., Caballero, O.L., et al. (2013). Targeting CXCL12 from FAP-expressing carcinoma-associated fibroblasts synergizes with anti-PD-L1 immunotherapy in pancreatic cancer. Proc. Natl. Acad. Sci. USA *110*, 20212–20217.

Fife, B.T., Pauken, K.E., Eagar, T.N., Obu, T., Wu, J., Tang, Q., Azuma, M., Krummel, M.F., and Bluestone, J.A. (2009). Interactions between PD-1 and PD-L1 promote tolerance by blocking the TCR-induced stop signal. Nat. Immunol. *10*, 1185–1192.

Fukuda, A., Wang, S.C., Morris, J.P., Folias, A.E., Liou, A., Kim, G.E., Akira, S., Boucher, K.M., Firpo, M.A., Mulvihill, S.J., and Hebrok, M. (2011). Stat3 and MMP7 contribute to pancreatic ductal adenocarcinoma initiation and progression. Cancer Cell *19*, 441–455.

Goldstein, D., El-Maraghi, R.H., Hammel, P., Heinemann, V., Kunzmann, V., Sastre, J., Scheithauer, W., Siena, S., Tabernero, J., Teixeira, L., et al. (2015). nab-Paclitaxel plus gemcitabine for metastatic pancreatic cancer: long-term survival from a phase III trial. J. Natl. Cancer Inst. *107*, http://dx.doi.org/10.1093/jnci/dju413.

Guerra, C., Schuhmacher, A.J., Canamero, M., Grippo, P.J., Verdaguer, L., Perez-Gallego, L., Dubus, P., Sandgren, E.P., and Barbacid, M. (2007). Chronic pancreatitis is essential for induction of pancreatic ductal adenocarcinoma by K-Ras oncogenes in adult mice. Cancer Cell *11*, 291–302.

Haeno, H., Gonen, M., Davis, M.B., Herman, J.M., Iacobuzio-Donahue, C.A., and Michor, F. (2012). Computational modeling of pancreatic cancer reveals kinetics of metastasis suggesting optimum treatment strategies. Cell *148*, 362–375.

Highfill, S.L., Cui, Y., Giles, A.J., Smith, J.P., Zhang, H., Morse, E., Kaplan, R.N., and Mackall, C.L. (2014). Disruption of CXCR2-mediated MDSC tumor trafficking enhances anti-PD1 efficacy. Sci. Transl Med. *6*, 237ra267.

Hingorani, S.R., Wang, L., Multani, A.S., Combs, C., Deramaudt, T.B., Hruban, R.H., Rustgi, A.K., Chang, S., and Tuveson, D.A. (2005). Trp53R172H and KrasG12D cooperate to promote chromosomal instability and widely metastatic pancreatic ductal adenocarcinoma in mice. Cancer Cell *7*, 469–483.

Hruban, R.H., Wilentz, R.E., and Kern, S.E. (2000). Genetic progression in the pancreatic ducts. Am. J. Pathol. *156*, 1821–1825.

Ijichi, H., Chytil, A., Gorska, A.E., Aakre, M.E., Bierie, B., Tada, M., Mohri, D., Miyabayashi, K., Asaoka, Y., Maeda, S., et al. (2011). Inhibiting Cxcr2 disrupts tumor-stromal interactions and improves survival in a mouse model of pancreatic ductal adenocarcinoma. J. Clin. Invest. *121*, 4106–4117.

Jacobetz, M.A., Chan, D.S., Neesse, A., Bapiro, T.E., Cook, N., Frese, K.K., Feig, C., Nakagawa, T., Caldwell, M.E., Zecchini, H.I., et al. (2013). Hyaluronan impairs vascular function and drug delivery in a mouse model of pancreatic cancer. Gut *62*, 112–120.

Jamieson, N.B., Glen, P., McMillan, D.C., McKay, C.J., Foulis, A.K., Carter, R., and Imrie, C.W. (2005). Systemic inflammatory response predicts outcome in patients undergoing resection for ductal adenocarcinoma head of pancreas. Br. J. Cancer *92*, 21–23.

Jamieson, T., Clarke, M., Steele, C.W., Samuel, M.S., Neumann, J., Jung, A., Huels, D., Olson, M.F., Das, S., Nibbs, R.J., and Sansom, O.J. (2012). Inhibition of CXCR2 profoundly suppresses inflammation-driven and spontaneous tumorigenesis. J. Clin. Invest. *122*, 3127–3144.

Kaneider, N.C., Agarwal, A., Leger, A.J., and Kuliopulos, A. (2005). Reversing systemic inflammatory response syndrome with chemokine receptor pepducins. Nat. Med. *11*, 661–665.

Kim, S., Takahashi, H., Lin, W.W., Descargues, P., Grivennikov, S., Kim, Y., Luo, J.L., and Karin, M. (2009). Carcinoma-produced factors activate myeloid cells through TLR2 to stimulate metastasis. Nature *457*, 102–106.

Kuilman, T., Michaloglou, C., Vredeveld, L.C., Douma, S., van Doorn, R., Desmet, C.J., Aarden, L.A., Mooi, W.J., and Peeper, D.S. (2008). Oncogene-induced senescence relayed by an interleukin-dependent inflammatory network. Cell *133*, 1019–1031.

Lal, A., Peters, H., St Croix, B., Haroon, Z.A., Dewhirst, M.W., Strausberg, R.L., Kaanders, J.H., van der Kogel, A.J., and Riggins, G.J. (2001). Transcriptional response to hypoxia in human tumors. J. Natl. Cancer Inst. *93*, 1337–1343.

Lesina, M., Kurkowski, M.U., Ludes, K., Rose-John, S., Treiber, M., Kloppel, G., Yoshimura, A., Reindl, W., Sipos, B., Akira, S., et al. (2011). Stat3/Socs3 activation by IL-6 transsignaling promotes progression of pancreatic intraepithelial neoplasia and development of pancreatic cancer. Cancer Cell *19*, 456–469.

Li, A., King, J., Moro, A., Sugi, M.D., Dawson, D.W., Kaplan, J., Li, G., Lu, X., Strieter, R.M., Burdick, M., et al. (2011). Overexpression of CXCL5 is associated with poor survival in patients with pancreatic cancer. Am. J. Pathol. *178*, 1340–1349.

Ling, J., Kang, Y., Zhao, R., Xia, Q., Lee, D.F., Chang, Z., Li, J., Peng, B., Fleming, J.B., Wang, H., et al. (2012). KrasG12D-induced IKK2/beta/NF-kappaB activation by IL-1alpha and p62 feedforward loops is required for development of pancreatic ductal adenocarcinoma. Cancer Cell *21*, 105–120.

Lowenfels, A.B., Maisonneuve, P., DiMagno, E.P., Elitsur, Y., Gates, L.K., Jr., Perrault, J., and Whitcomb, D.C. (1997). Hereditary pancreatitis and the risk of pancreatic cancer. International hereditary pancreatitis study group. J. Natl. Cancer Inst. *89*, 442–446.

Maniati, E., Bossard, M., Cook, N., Candido, J.B., Emami-Shahri, N., Nedospasov, S.A., Balkwill, F.R., Tuveson, D.A., and Hagemann, T. (2011). Crosstalk between the canonical NF-kappaB and Notch signaling pathways inhibits Pparγ expression and promotes pancreatic cancer progression in mice. J. Clin. Invest. *121*, 4685–4699.

Matsuo, Y., Ochi, N., Sawai, H., Yasuda, A., Takahashi, H., Funahashi, H., Takeyama, H., Tong, Z., and Guha, S. (2009a). CXCL8/IL-8 and CXCL12/SDF-1alpha co-operatively promote invasiveness and angiogenesis in pancreatic cancer. Int. J. Cancer *124*, 853–861.

Matsuo, Y., Raimondo, M., Woodward, T.A., Wallace, M.B., Gill, K.R., Tong, Z., Burdick, M.D., Yang, Z., Strieter, R.M., Hoffman, R.M., and Guha, S. (2009b). CXC-chemokine/CXCR2 biological axis promotes angiogenesis in vitro and in vivo in pancreatic cancer. Int. J. Cancer *125*, 1027–1037.

Morton, J.P., Karim, S.A., Graham, K., Timpson, P., Jamieson, N., Athineos, D., Doyle, B., McKay, C., Heung, M.Y., Oien, K.A., et al. (2010). Dasatinib

inhibits the development of metastases in a mouse model of pancreatic ductal adenocarcinoma. Gastroenterology *139*, 292–303.

Nicholls, D.J., Wiley, K., Dainty, I., MacIntosh, F., Phillips, C., Gaw, A., and Mardh, C.K. (2015). Pharmacological characterization of AZD5069, a slowly reversible CXC chemokine receptor 2 antagonist. J. Pharmacol. Exp. Ther. *353*, 340–350.

Olive, K.P., Jacobetz, M.A., Davidson, C.J., Gopinathan, A., McIntyre, D., Honess, D., Madhu, B., Goldgraben, M.A., Caldwell, M.E., Allard, D., et al. (2009). Inhibition of Hedgehog signaling enhances delivery of chemotherapy in a mouse model of pancreatic cancer. Science *324*, 1457–1461.

Oskarsson, T., Acharyya, S., Zhang, X.H., Vanharanta, S., Tavazoie, S.F., Morris, P.G., Downey, R.J., Manova-Todorova, K., Brogi, E., and Massague, J. (2011). Breast cancer cells produce tenascin C as a metastatic niche component to colonize the lungs. Nat. Med. *17*, 867–874.

Ozdemir, B.C., Pentcheva-Hoang, T., Carstens, J.L., Zheng, X., Wu, C.C., Simpson, T.R., Laklai, H., Sugimoto, H., Kahlert, C., Novitskiy, S.V., et al. (2014). Depletion of carcinoma-associated fibroblasts and fibrosis induces immunosuppression and accelerates pancreas cancer with reduced survival. Cancer Cell *25*, 719–734.

Provenzano, P.P., Cuevas, C., Chang, A.E., Goel, V.K., Von Hoff, D.D., and Hingorani, S.R. (2012). Enzymatic targeting of the stroma ablates physical barriers to treatment of pancreatic ductal adenocarcinoma. Cancer Cell *21*, 418–429.

Purohit, A., Varney, M., Rachagani, S., Ouellette, M.M., Batra, S.K., and Singh, R.K. (2016). CXCR2 signaling regulates KRAS(G12D)-induced autocrine growth of pancreatic cancer. Oncotarget *7*, 7280–7296.

Reid, M.D., Basturk, O., Thirabanjasak, D., Hruban, R.H., Klimstra, D.S., Bagci, P., Altinel, D., and Adsay, V. (2011). Tumor-infiltrating neutrophils in pancreatic neoplasia. Mod. Pathol. *24*, 1612–1619.

Rhim, A.D., Mirek, E.T., Aiello, N.M., Maitra, A., Bailey, J.M., McAllister, F., Reichert, M., Beatty, G.L., Rustgi, A.K., Vonderheide, R.H., et al. (2012). EMT and dissemination precede pancreatic tumor formation. Cell *148*, 349–361.

Rhim, A.D., Oberstein, P.E., Thomas, D.H., Mirek, E.T., Palermo, C.F., Sastra, S.A., Dekleva, E.N., Saunders, T., Becerra, C.P., Tattersall, I.W., et al. (2014). Stromal elements act to restrain, rather than support, pancreatic ductal adenocarcinoma. Cancer Cell *25*, 735–747.

Saintigny, P., Massarelli, E., Lin, S., Ahn, Y.H., Chen, Y., Goswami, S., Erez, B., O'Reilly, M.S., Liu, D., Lee, J.J., et al. (2013). CXCR2 expression in tumor cells is a poor prognostic factor and promotes invasion and metastasis in lung adenocarcinoma. Cancer Res. *73*, 571–582.

Sharma, P., and Allison, J.P. (2015). The future of immune checkpoint therapy. Science *348*, 56–61.

Siegel, R.L., Miller, K.D., and Jemal, A. (2015). Cancer statistics, 2015. CA Cancer J. Clin. *65*, 5–29.

Steele, C.W., Karim, S.A., Foth, M., Rishi, L., Leach, J.D., Porter, R.J., Nixon, C., Jeffry Evans, T.R., Carter, C.R., Nibbs, R.J., et al. (2015). CXCR2 inhibition suppresses acute and chronic pancreatic inflammation. J. Pathol. *237*, 85–97.

Stromnes, I.M., Brockenbrough, J.S., Izeradjene, K., Carlson, M.A., Cuevas, C., Simmons, R.M., Greenberg, P.D., and Hingorani, S.R. (2014). Targeted depletion of an MDSC subset unmasks pancreatic ductal adenocarcinoma to adaptive immunity. Gut *63*, 1769–1781.

Stromnes, I.M., Schmitt, T.M., Hulbert, A., Brockenbrough, J.S., Nguyen, H.N., Cuevas, C., Dotson, A.M., Tan, X., Hotes, J.L., Greenberg, P.D., and Hingorani, S.R. (2015). T cells engineered against a native antigen can surmount immunologic and physical barriers to treat pancreatic ductal adenocarcinoma. Cancer Cell *28*, 638–652.

Wang, S., Wu, Y., Hou, Y., Guan, X., Castelvetere, M.P., Oblak, J.J., Banerjee, S., Filtz, T.M., Sarkar, F.H., Chen, X., et al. (2013). CXCR2 macromolecular complex in pancreatic cancer: a potential therapeutic target in tumor growth. Transl Oncol. *6*, 216–225.

Wculek, S.K., and Malanchi, I. (2015). Neutrophils support lung colonization of metastasis-initiating breast cancer cells. Nature *528*, 413–417.

Winograd, R., Byrne, K.T., Evans, R.A., Odorizzi, P.M., Meyer, A.R., Bajor, D.L., Clendenin, C., Stanger, B.Z., Furth, E.E., Wherry, E.J., and Vonderheide, R.H. (2015). Induction of T-cell immunity overcomes complete resistance to PD-1 and CTLA-4 blockade and improves survival in pancreatic carcinoma. Cancer Immunol. Res. *3*, 399–411.

Yan, H.H., Pickup, M., Pang, Y., Gorska, A.E., Li, Z., Chytil, A., Geng, Y., Gray, J.W., Moses, H.L., and Yang, L. (2010). Gr-1+CD11b+ myeloid cells tip the balance of immune protection to tumor promotion in the premetastatic lung. Cancer Res. *70*, 6139–6149.

Yang, L., Huang, J., Ren, X., Gorska, A.E., Chytil, A., Aakre, M., Carbone, D.P., Matrisian, L.M., Richmond, A., Lin, P.C., and Moses, H.L. (2008). Abrogation of TGF beta signaling in mammary carcinomas recruits Gr-1+CD11b+ myeloid cells that promote metastasis. Cancer Cell *13*, 23–35.

Youn, J.I., and Gabrilovich, D.I. (2010). The biology of myeloid-derived suppressor cells: the blessing and the curse of morphological and functional heterogeneity. Eur. J. Immunol. *40*, 2969–2975.

Cancer Cell, Volume *29*

Supplemental Information

CXCR2 Inhibition Profoundly Suppresses Metastases and Augments Immunotherapy in Pancreatic Ductal Adenocarcinoma

Colin W. Steele, Saadia A. Karim, Joshua D.G. Leach, Peter Bailey, Rosanna Upstill-Goddard, Loveena Rishi, Mona Foth, Sheila Bryson, Karen McDaid, Zena Wilson, Catherine Eberlein, Juliana B. Candido, Mairi Clarke, Colin Nixon, John Connelly, Nigel Jamieson, C. Ross Carter, Frances Balkwill, David K. Chang, T.R. Jeffry Evans, Douglas Strathdee, Andrew V. Biankin, Robert J.B. Nibbs, Simon T. Barry, Owen J. Sansom, and Jennifer P. Morton

Supplemental Data

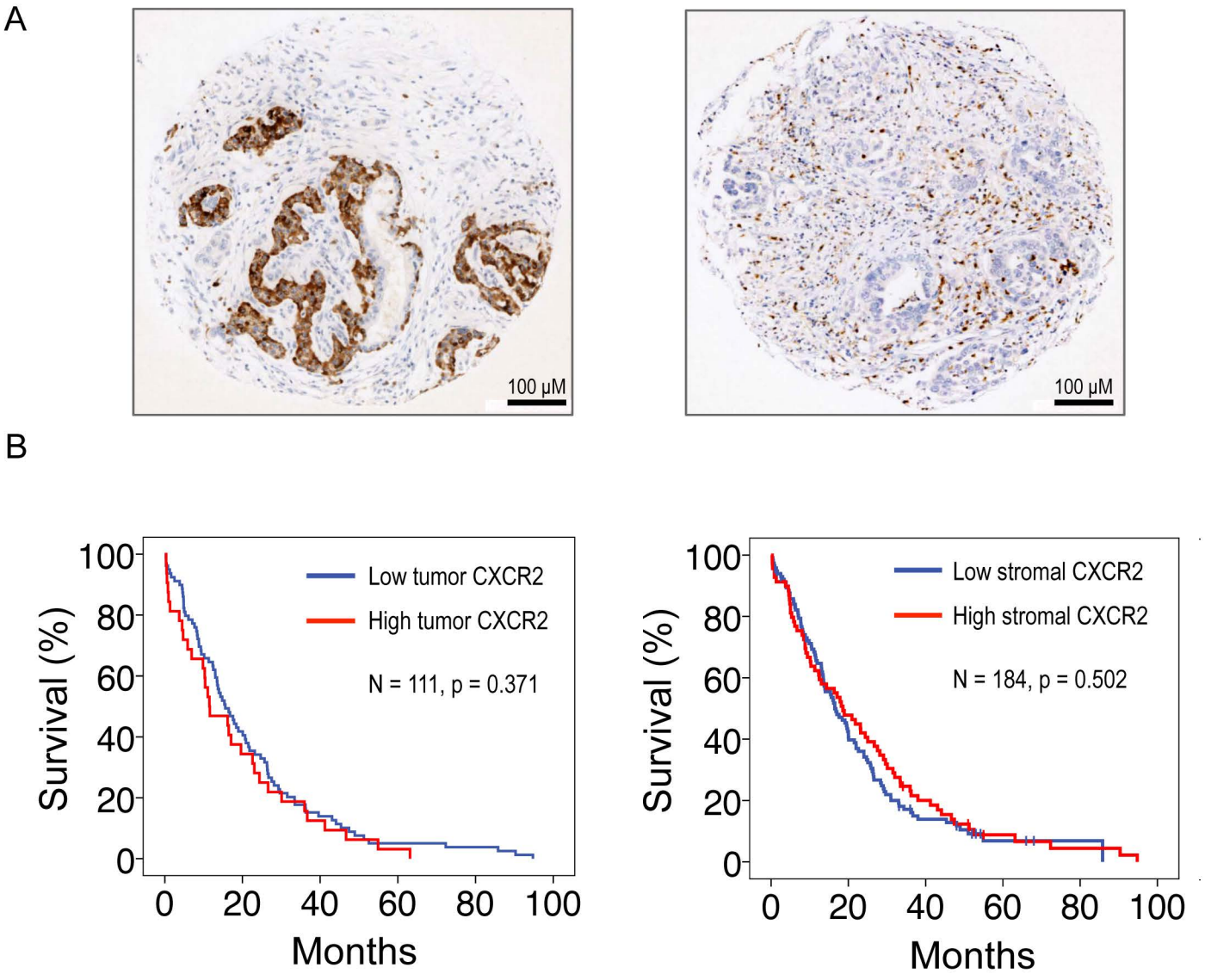

Figure S1, related to Figure 1

The effects of CXCR2 signaling in pancreatic tumors are dependent on location
(A) IHC for CXCR2 on a human pancreatic cancer TMA. The left image is representative of tumor epithelium scored as 'high'. The right image is representative of tumor stroma scored as 'high'. (B) Kaplan-Meier analyses of patient survival stratified on high and low tumor cell CXCR2 expression and high and low stromal expression, p value, Log Rank.

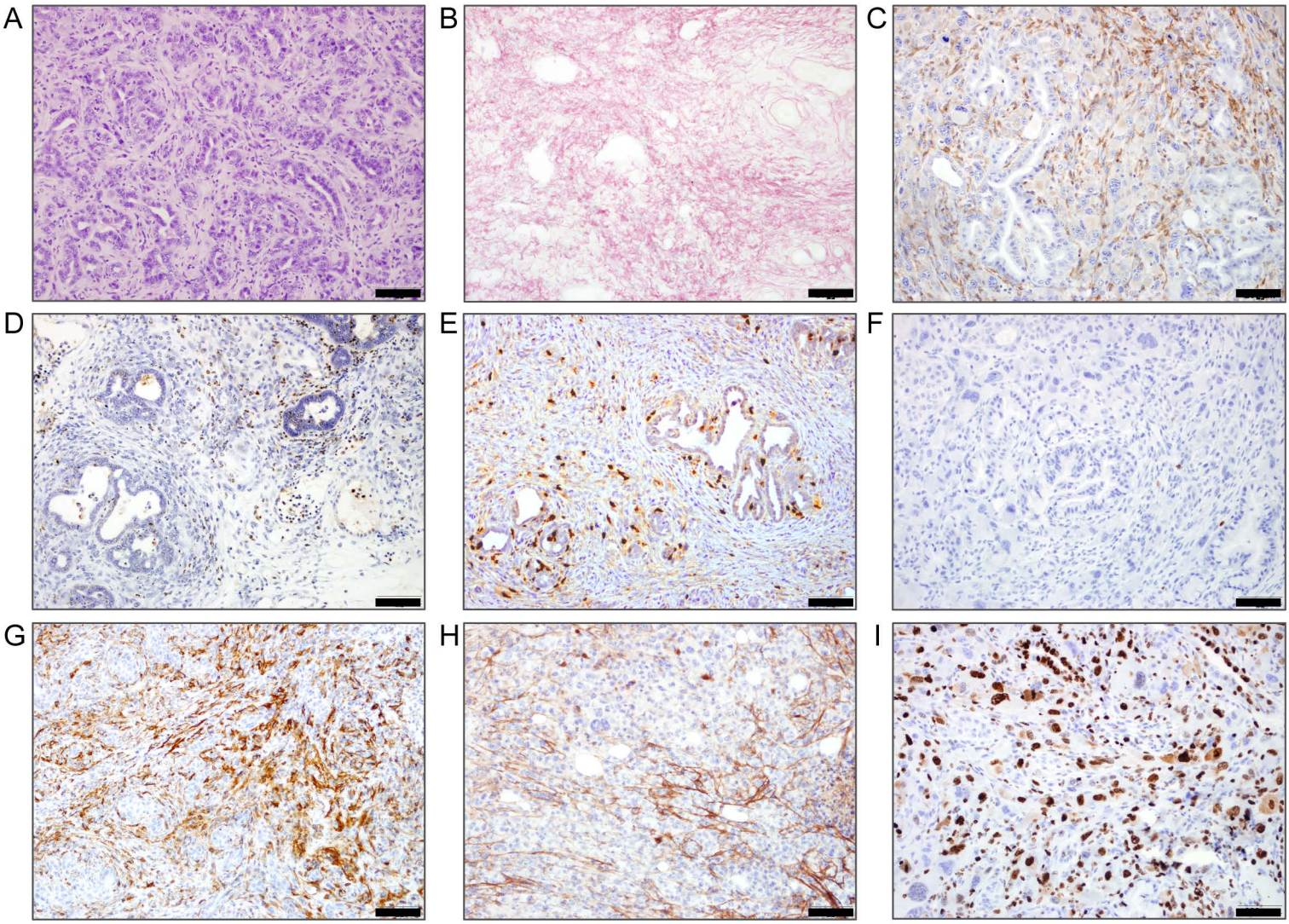

Figure S2, related to Figure 2

Stromal characterization of KPC PDAC
(A) H&E, (B) Picrosirius red staining (collagen) (C-I) IHC for (C) F4/80 (macrophages), (D) MPO (neutrophils and precursors), (E) S100A9 (neutrophil precursors, BMDCs), (F) CD3 (T cells), (G) αSMA (activated fibroblasts), (H) Tenascin C, and I) Ki67. Scale bars = 200 μM.

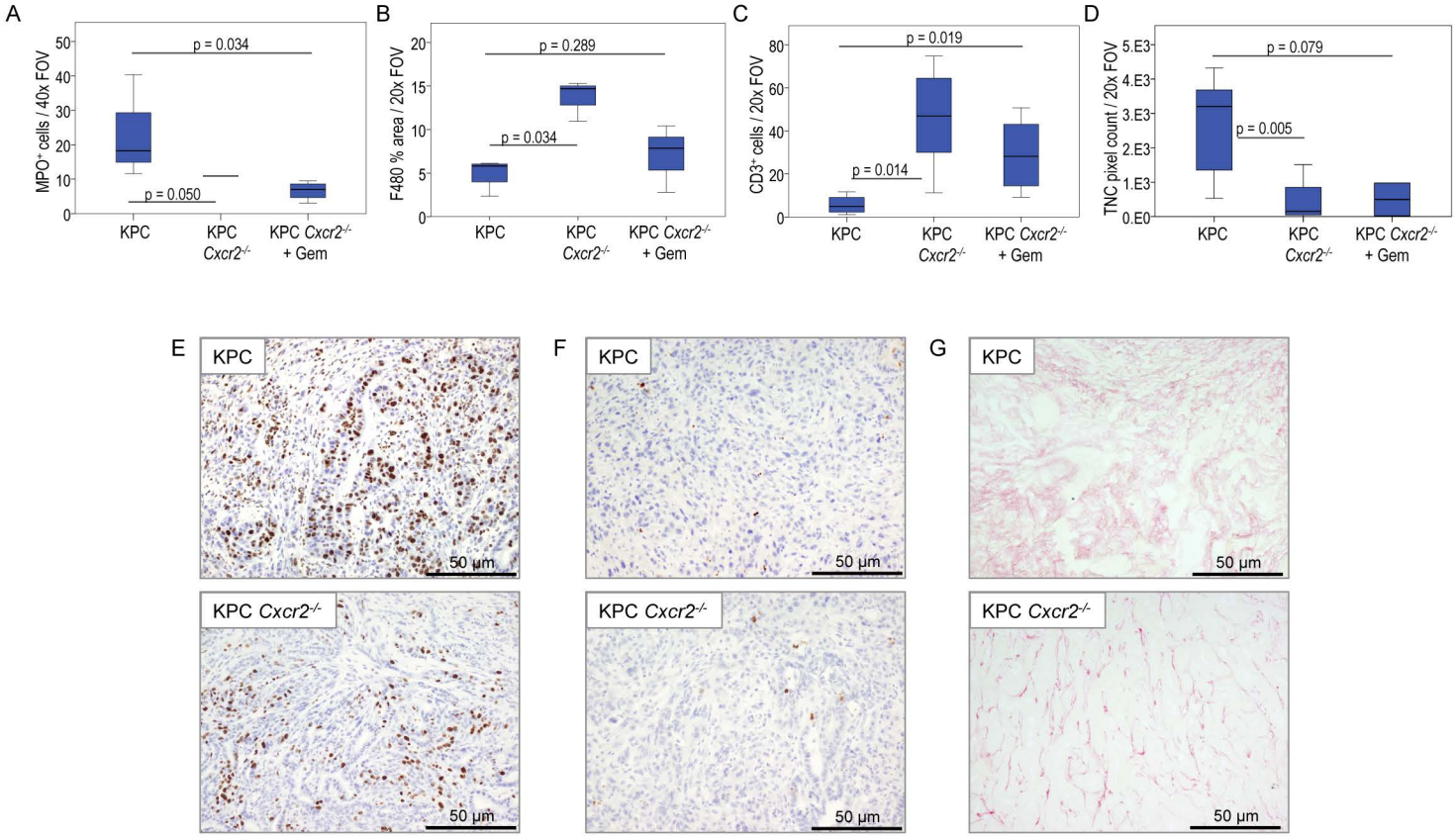

Figure S3, related to Figure 3

Effects of Cxcr2 deletion on stromal markers within the primary tumor
(A-D) Boxplots showing quantification of (A) MPO IHC, (B) F4/80 IHC, (C) CD3 IHC, and (D) Tenascin C IHC in tumors from KPC and KPC *Cxcr2*$^{-/-}$ mice treated as indicated. p values, Mann Whitney, n ≥ 3. Note that there is no box, and only a median line for MPO^{+} cells in KPC *Cxcr2*$^{-/-}$ mice because all the tumors assessed had the same score. (E-G) IHC for (E) Ki67, (F) cleaved caspase 3, and (G) picrosirius red, in tumors from KPC or KPC *Cxcr2*$^{-/-}$ mice as indicated.

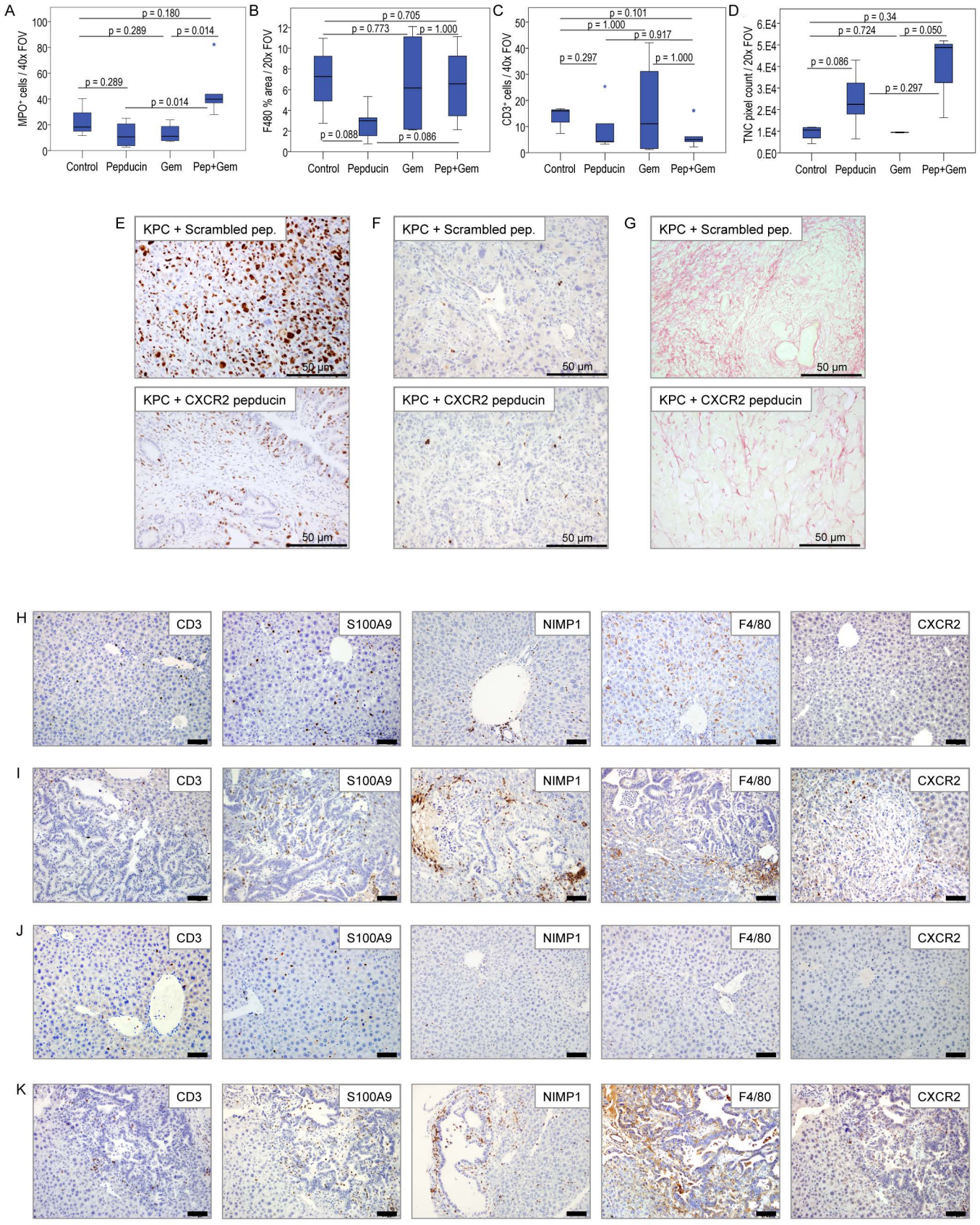

Figure S4, related to Figure 5

Effects on stromal markers within the primary tumor and liver in response to CXCR2-inhibiting pepducin

(A-D) Boxplots showing quantification of (A) MPO IHC, (B) F4/80 IHC, (C) CD3 IHC, and (D) Tenascin C IHC in tumors from KPC mice treated with scrambled pepducin, CXCR2-inhibiting pepducin, gemcitabine or CXCR2-pepducin combined with gemcitabine as indicated. P values, Mann Whitney, n ≥ 3. (E-G) IHC for (E) Ki67, (F) cleaved caspase 3, and (G) picrosirius red, in tumors from KPC mice treated with scrambled pepducin or CXCR2-inhibiting pepducin. (H-K) IHC for CD3, S100A9, NIMP1 (neutrophils), F4/80 and CXCR2, as indicated, in (H) pre-metastatic livers of KPC mice, (I) KPC liver metastases, (J) the livers of KPC mice treated with CXCR2 pepducin and gemcitabine from 10 weeks of age, and (K) the livers of KPC mice treated with CXCR2 pepducin and gemcitabine once symptoms are apparent. Scale bars = 200 µM.

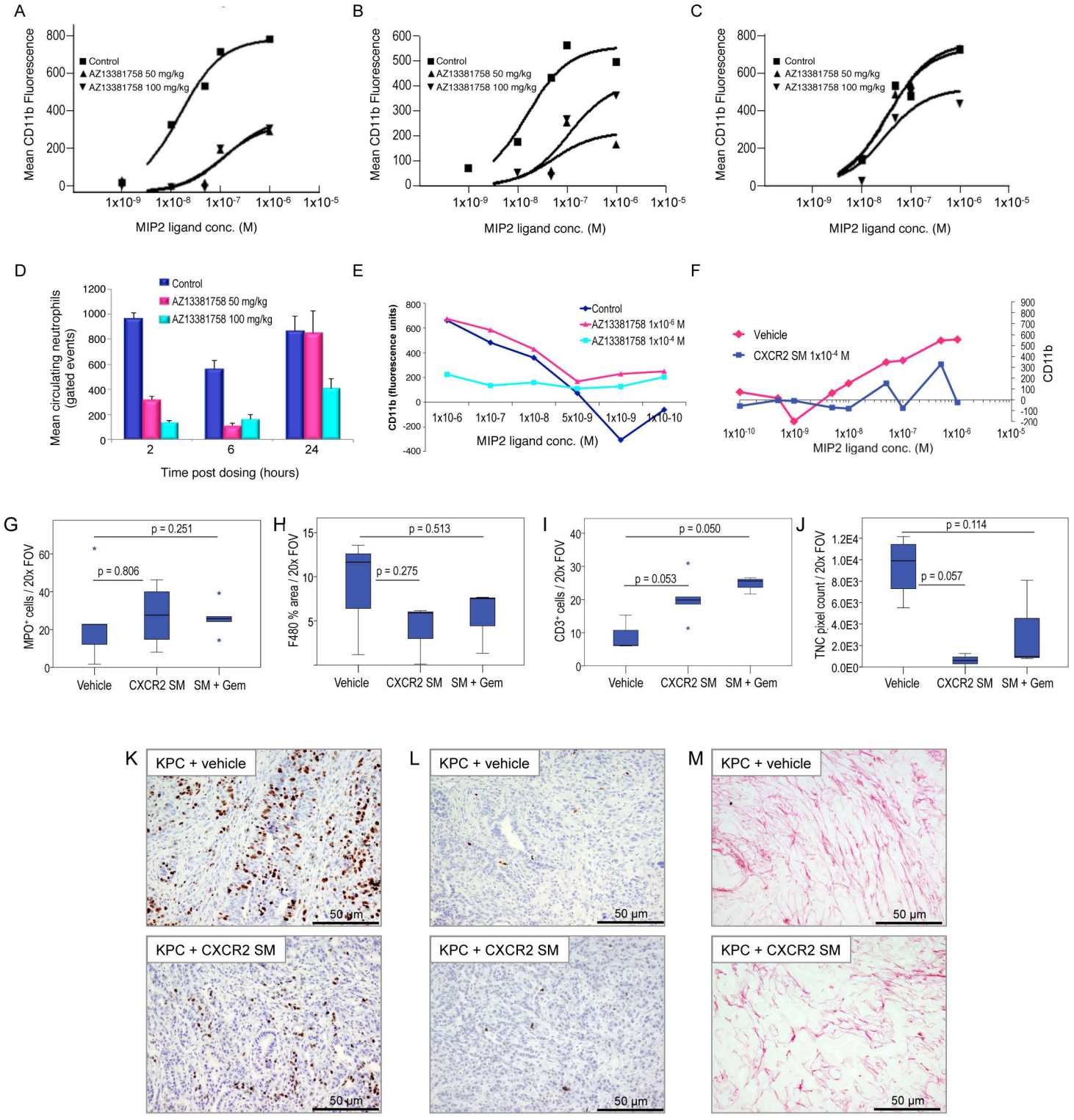

Figure S5, related to Figure 6

Validation of AZ13381758 (CXCR2 SM) and its effects on stromal markers in primary tumors
(A-C) MIP2 ligand-stimulated CD11b expression in blood from C57Bl/6 mice (A) 2 hours, (B) 6 hours, or (C) 24 hours following a single dose of CXCR2 antagonist AZ13381758 at 50 mg/kg or 100 mg/kg. (D) Mean number of circulating neutrophils following a single bolus dose of AZ13381758 in C57Bl/6 mice treated as indicated, n=3. (E) Quantification of MIP2–CXCR2-induced stimulation of CD11b expression on neutrophils ex vivo (performed 15 minutes after AZ13381758 was spiked into whole blood pooled from 10 mice). F) Blood neutrophil depletion in pooled whole blood from CXCR2 SM treated KPC mice. Recombinant MIP2 was added followed by anti-CD11b antibody and the number of CD11b-expressing cells determined by flow cytometry. (G-J) Boxplots showing quantification of (G) MPO IHC, (H) F4/80 IHC, (I) CD3 IHC, and (J) Tenascin C IHC in tumors from KPC mice treated with vehicle, CXCR2 SM, or CXCR2 SM in combination with gemcitabine as indicated. P values, Mann Whitney, n ≥ 3. (K-M) IHC for (L) Ki67, (L) cleaved caspase 3, and (M) picrosirius red, in tumors from KPC mice treated with vehicle, CXCR2 SM, or CXCR2 SM in combination with gemcitabine as indicated.

Table S1, related to Figure 6

In vitro potency of AZ13381758 versus mCXCR2 and hCXCR2

Species	Compounds		
	hCXCR2 antibody (HY29) (µg/ml)	mCXCR2 antibody (18-74-5) (µg/ml)	AZ13381758 (µM)
mCXCR2	>10 ± 0	0.44 ± 0	0.026 ± 0
hCXCR2	0.74 ± 0.129	>10 ± 0	0.03 ± 0.001

Values = mean IC50 ± std dev (n = 2)

Supplemental Experimental Procedures

Human Pancreatic Cancer Microarray

Tissue microarrays containing at least 3 cores of resected PDAC from each of 184 patients with full clinicopathological data were obtained from Glasgow Biorepository. Tissue was collected prospectively with local ethical approval and fully informed consent. Following immunohistochemistry, expression was scored using a weighted histoscore (= Σ(0 x % unstained) + (1 x % low) + (2 x % medium) + (3 x % high)).

Human Gene Expression Analysis

Fresh frozen PDAC tissue samples were obtained from 47 patients undergoing pancreaticoduodenectomy at the West of Scotland Pancreatic Unit and macrodissected to acquire samples from tumor border and adjacent normal tissue. Tissue was collected prospectively with local ethical approval and fully informed consent. Only histologically proven PDACs were included. Complete clinicopathological, follow-up and recurrence data were available. RNA was isolated from frozen tissue by TRIzol (Invitrogen) extraction according to the manufacturer's instructions. Samples with a RNA integrity number (RIN) above 7.0 were selected for downstream analysis. Transcript profiling was performed as described previously (GEO GSE55643). Kaplan-Meier survival analysis was used to analyze overall survival from time of surgery. A Log Rank test was used to compare length of survival between curves. Statistical significance was set at a p value of < 0.05. All statistical analyses were performed using SPSS version 19.0 (Version 19.0. Armonk, NY: IBM Corp.)

Immunohistochemistry

IHC was performed on formalin fixed paraffin embedded pancreatic tissue using standard protocols. Quantification was performed using visual counts at x20 or x40 fields of view using an Olympus BX53 microscope (where possible, >30 fields per animal). To quantify stromal stains, pictures were taken of >30 fields of view at x40 magnification, and Adobe Photoshop 5.1 used to pixel count the positive staining.

Immunohistochemistry Antibodies:

Protein	**Clone**	**Conc.**	**Supplier**
MPO		1/200	Dako A0398
F4/80	A3-1	1/400	Abcam ab6640
CD3	SP7	1/75	Vector VP-RM01
Ki67	SP6	1/200	Thermo RM-9106
Cleaved Caspase 3	ASP175	1/50	Cell Signaling 9661
CXCR2	19 242216	1/200 1/500	Human: Invitrogen AHR1532X Mouse: R&D systems MAB2164-100
CXCL2	40605	1/200	R&D systems MAB452
CXCL1		1/100	AbCam ab86436
αSMA	1A4	1/20000	Sigma-Aldrich A2547
CK19	A53-B	1/500	AbCam ab194399
1A8	1A8	1/500	Biolegend 127602
Tenascin C	M-Tn12	1/1000	Sigma-Aldrich T3413
Nimp1	NIMP-R14	1/50	Abcam ab2557
S100A9/Calgranulin	M-19	1/1000	Santa Cruz sc-8115

Animal Experiments

All animal experiments were performed under UK Home Office licence and approved by the local ethics committee. Mice were maintained in conventional cages and given access to standard diet and water ad libitum. Mice were genotyped by Transnetyx (Cordoba, TN, USA). *Cxcr2*$^{-/-}$ mice on a *BALB/c* background were obtained from The Jackson Laboratory (Cacalano et al., 1994). KPC mice were first described by (Hingorani et al., 2005) and were bred in house on a mixed background. Mice were monitored at least 3 times weekly and culled when exhibiting symptoms of PDAC. For short term drug studies pancreatic malignancy was confirmed by abdominal palpation.

Laser Capture Microdissection

Primary pancreatic tumors were dissected from mice, snap frozen, and mounted in optimal cutting temperature (OCT) cryostat compound. 35 μM sections were cut from these tumors and stained with crystal violet. Using Leica microdissection microscope LMD 6500 areas of tumor and stroma were dissected and tissue immediately snap frozen and RNA extracted.

RNA Extraction

Portions of murine pancreatic tumors were frozen in RNAlater (Qiagen) solution until required. LCM RNA was snap frozen. RNA extraction was performed using Qiagen RNeasy Plus Mini Kit (Qiagen) and homogenized in a Precellys with ceramic beads (Stretton scientific). DNA was removed with Turbo DNA-*free* Kit (Applied

Biosystems). RNA integrity was assessed using Agilent 2100 Bioanalyzer in conjunction with RNA 6000 Nano LabChip kits (Agilent).

qPCR

SYBR Green qPCR kits (Thermo Scientific) were utilized to perform real time PCR for *Cxcr2* and its ligands *Cxcl1*, *Cxcl2*, and *Cxcl5*. cDNA was prepared from mouse total RNA using standard protocols. qPCR was performed using these primers:

CXCL1 F: 5' CTGGGATTCACCTCAAGAACATC

CXCL1 R: 5' CAGGGTCAAGGCAAGCCTC

CXCL2 F: 5' CCAACCACCAGGCTACAGG

CXCL2 R: 5' GCGTCACACTCAAGCTCTG

CXCL5 F: 5' GTTCCATCTCGCCATTCATGC

CXCL5 R: 5' GCGGCTATGACTGAGGAAGG

CXCR2 F: 5' ATGCCCTCTATTCTGCCAGAT

CXCR2 R: 5' GTGCTCCGGTTGTATAAGATGAC

Opticon monitor software (Bio-Rad) was used for data collection and analysis. All PCR products were analyzed in the exponential phase of amplification. Quantification of the relative expression of *Cxcr2* and its ligands transcripts was performed using standard curves normalized to *Gapdh* transcripts.

mRNASeq analysis

Sequencing was done by Source BioScience using Illumina TruSeq RNA library preparation, and Illumina HiSeq sequencing and HiSeq2000 analysis. Reads were

analysed using the *bcbio-nextgen* framework (https://bcbio-nextgen.readthedocs.org/en/latest/). After quality control and adaptor trimming, reads were aligned to the UCSC mouse mm10 genome build using STAR Counts for known genes were generated using the function *featureCounts* in the R/Bioconductor package "Rsubread". The R/Bioconductor package "edgeR" was used to identify differentially expressed genes.

Cxcr2$^{-/-}$ signature PDAC subtype enrichment

To determine the enrichment of *Cxcr2*$^{-/-}$ differentially expressed mouse genes in PDAC subtypes, mouse identifiers were first mapped to their corresponding human HGCN Symbol using the R/Bioconductor package "biomaRt". After mapping, gene set enrichment in PDAC was performed using the R package 'GSVA' (function gsva - arguments: method="gsva", mx.diff=TRUE). GSVA implements a non-parametric unsupervised method of gene set enrichment that allows an assessment of the relative enrichment of a selected pathway across the sample space. The output of GSVA is a gene-set by sample matrix of GSVA enrichment scores. GSVA enrichment scores were generated exclusively for both upregulated and downregulated genes using transformed count data and stratified on the basis of subtype. A Kruskal-Wallis test was applied to the stratified scores to determine whether the distributions were significantly different.

Efficacy testing of CXCR2 small molecule inhibitor (AZ13381758)

In vitro: HEK 293s Gqi5 cells over-expressing murine or human CXCR2 receptor were cultured in DMEM + Glutamax (Invitrogen), 10% FCS, 1000 µg/ml G418, 300 µg

Hygromycin B. 24 hours before the assay, cells were plated in black 384 well poly-D-lysine coated plates at 12000 cells per well in 70 µl growth media / well and grown overnight at 37 °C in a CO_2 incubator. The following day the cells were loaded with Calcium 3 dye (Molecular devices) and Fluo-4 AM stocks (Invitrogen) for 30 minutes at 37 °C at room temperature, treated with AZ13381758 and then stimulated with MIP2 (R&D Systems) at 0.5 mg/ml. Species selectivity of each assay was demonstrated using therapeutic antibodies HY29 and 18-74-5 that block human and murine receptor respectively.

In vivo: Non tumour bearing female C57BL/6J mice (Harlan UK) were dosed with a single oral bolus of AZ13381758, n = 3 mice per treatment group. Animals were terminated using rising levels of CO_2, and terminal blood samples were slowly taken via vena cava into lithium-heparin tubes. Whole blood (80 µl) was placed into polypropylene tubes. A range of concentrations of 10 µl recombinant MIP2 (R&D Systems) was added followed by 10 µl of PE-labeled rat anti-mouse CD11b antibody (Serotec). Following 40 minutes incubation in the dark at room temperature the tubes were placed on ice. The cells were processed using Immunoprep (Beckman Coulter) to lyse red blood cells and fix leukocytes. The level of CD11b expression was determined using a Becton Dickinson Facs Caliber. Neutrophils were gated based on their forward scatter / side scatter profile.

Ex vivo: AZ13381758 was spiked into whole murine blood pooled from 10 mice and incubated at room temperature for 15 minutes before the CD11b assay was performed.

Flow Cytometry

Tumours were minced and incubated at 37 °C for 20-30 minutes in an enzymatic cocktail (Dnase (0.5 mg/ml, Sigma) and collagenase type V (2 mg/ml, Sigma) in RPMI 1640 (Sigma) to make a single cell suspension. This was passed through a 70 μM filter (BD Biosciences), washed in PBS supplemented with 2% foetal bovine serum and 2 mM EDTA, counted and used immediately for flow cytometry. Flow cytometry was performed with the antibodies listed below. All surface staining were performed in in PBS supplemented with 2% foetal bovine serum and 2 mM EDTA. Fixable viability dye (eBioscience) was used to discriminate between live and dead cells. Acquisition and analyses were performed on a BD LSRII system using BD FACSDIVA software (BD Biosciences). Collected data were analysed using FlowJo software (version 10.0.7r2 tree Star). Cells were gated based on CD45 positivity, followed by CD3, CD4/8 and CD62L/CD44.

Antibody	**Fluorochrome**	**Clone**	**Vendor**
CD45	BV (Brilliant Violet) 570	30-F11	Biolegend
CD3	PE-Cyanine 7	145-2C11	Biolegend
CD4	APC (allophycocyanin)	RM4-5	eBioscience
CD8	PE (phycoerythrin)	53-6.7	eBioscience
CD44	BV650	IM7	Biolegend
CD62L	BV605	MEL-14	Biolegend
PD1	eFluor450	RMP1-30	eBioscience